Non-intrusive bridge weigh-in-motion: Integrating geophones and strain sensors for accurate vehicle characterization.

By

Taimur Ishtiaq

A Thesis submitted to the Faculty of Graduate Studies of

The University of Manitoba

in partial fulfillment of the requirements of the degree of

MASTER OF SCIENCE

Department of Civil Engineering

University of Manitoba

Winnipeg

ABSTRACT

This study introduces an innovative Bridge Weigh-in-Motion (BWIM) approach, utilizing a geophone, a novel sensor in the field of Structural Health Monitoring (SHM). Vehicle overloading poses a serious threat to bridge safety and service life. Loaded vehicles exert excessive stress on bridge decks, road pavements, and girders, leading to accelerated degradation of bridge structural components. Therefore, accurate information regarding real traffic loads, especially heavy vehicles, is critical for assessing bridge health. The proposed BWIM system combines geophones and strain sensors to accurately determine axle loads, axle spacing, and Gross Vehicle Weight (GVW) in regular traffic flow. The research methodology consists of bridge span instrumentation, data acquisition, processing, storage, and analysis, detailing the methods for extracting vehicle characteristics from measured bridge responses. Validation is done with field experiments on a real instrumented bridge in Winnipeg, Canada. This study focuses on loaded trucks. Velocity measurements exhibited an error range of -5% to 3.8%, with a confident 95% interval of -0.4% to 0.54% and an R2 value of 0.95, based on a sample of 64 vehicles. GVW calculations demonstrated an error range of -4.6% to +3.2%, and 95% confidence interval of -2.7% to 3.2%, derived from 6 runs of known GVWs. Axle detection accuracy was 95%, assessed across a sample of 41 trucks exceeding 150 kN in GVW. Axle spacings and loads were calculated in the error ranges of -10.52% to 7.8% and -4.97% to 10.48%, respectively. Confidence intervals for these metrics ranged from -2.4% to 3.2% and 1.05% to 8.6%, respectively. This study offers a contribution to the domain of SHM and Civionics, providing a reliable solution for axle detection of loaded trucks and assessing real traffic loads on instrumented bridges.

ACKNOWLEDGEMENTS

I would like to express my deepest gratitude to all those who have contributed to the completion of this research and the writing of this thesis. First and foremost, I am immensely grateful to my advisors, Dr. Aftab Mufti and Dr. Douglas Thomson, for their guidance, expertise, and unwavering support throughout the entire research process. Their invaluable insights, constructive feedback, and encouragement have been instrumental in shaping the direction and quality of this work.

I would like to extend my sincere appreciation to the members of my committee, Dr. Baidar Bakht and Dr. Jonathan Regehr for their valuable input and insightful comments. I would also like to thank the faculty and staff of the Department of Civil Engineering at the University of Manitoba for providing a conducive academic environment and access to necessary resources. I would like to express my profound gratitude to my lab colleagues, Dr. Basheer Algohi and Maedeh Mirzaei, for their invaluable contributions.

I would like to acknowledge the financial support received through the University of Manitoba Graduate Fellowship (UMGF) and JMBT – Vector Scholarship for research in Civionics Engineering.

Finally, I would like to thank all my family members especially my father Ishtiaq, mother Olga and sister Naila for their constant encouragement and support that has kept me motivated throughout the years.

CONTENTS

LIST OF TABLES

LIST OF FIGURES

1 INTRODUCTION

1.1 Motivation

Vehicles exceeding normal weight limitations are one of the major global concerns for the safety and service life of bridges (Law et al. 2004). Loaded vehicles pose an increased risk of damaging the infrastructure (Jacob et al. 2010). As these vehicles pass over bridges, the axel loads can damage bridge decks and road pavements (Haghani et al. 2012). The total weight of a vehicle, i.e., the Gross Vehicle Weight (GVW), affects the load carrying capacity of most components of bridges, including the fatigue of bridge girders (Archilla et al. 2000). The wheel loads affect the life of pavements and some components of bridges, such as concrete deck slabs of girder bridges. Therefore, accurate information about the GVW and axle weights of all vehicles is crucial for understanding the current health of bridges (Lydon et al. 2016). This information facilitates well-informed maintenance, planning, and budgeting strategies, ultimately ensuring the long-term structural integrity and safety of bridges, as well as extending their service life and increasing the confidence in their safety. Given the inherent variability in traffic loading patterns across different bridges, accurately assessing bridge conditions becomes a complex task, often resulting in either unnecessary costly repairs or an overestimation of safety measures (Lydon et al. 2016).

Accurate determination of the GVW through bridge weighing in motion (BWIM) has been around for quite some time (Helmi et al., 2014). However, the degree of error in determining axle weights and their spacing through BWIM has so far been quite large. This thesis introduces an innovative technology that uses a combination of geophone and strain sensors to determine more accurately the axle loads of vehicles passing over an instrumented bridge span at regular traffic speeds. Furthermore, this study enables future expansion to extend this system for even higher accuracy and enhanced algorithms.

1.2 Background and context

The monitoring of bridges through instruments has been a significant area of research for many decades. Researchers have proposed diverse techniques, utilizing a range of sensors such as strain gauges, accelerometers, load cells, piezoelectric sensors, acoustic sensors, and more, to analyze the dynamic response of bridges to traffic loads. Over time, various technologies have emerged, with early methods involving static weighing on stationary scales and Weigh-In-Motion (WIM) techniques.

Static weighing requires trucks to stop at a weighing station, causing unnecessary delays. WIM, on the other hand, deploys sensors cut into the pavement, often exhibiting poor durability, and causing traffic disruptions during installation and maintenance. Recently, there has been a surging interest in non-intrusive bridge monitoring methods that avoid disrupting traffic flow and potentially offer more precise measurements (Rashidi et al. 2020). This interest has given rise to the proposal of the Bridge Weigh-In-Motion (BWIM) system as an alternative (e.g., Moses et al. 1979; and Helmi et al, 2014).

B-WIM utilizes instrumented bridges as weighing scales to compute vehicle weights within regular traffic flow. A complete BWIM system consists of sensors mounted beneath the bridge, a data acquisition system for recording data, a communication system facilitating interaction or data transmission, and computer algorithms designed to analyze the collected data. Despite the development of various sensor configurations and algorithms for BWIM to determine Gross

Vehicle Weight (GVW) and axle loads, the accurate detection of axle weights remains a significant challenge.

The primary hurdle in BWIM is the accurate measurement of axle loads. While Literature Review provides an in-depth insight, a key issue is that the algorithms for axle load measurement require precise knowledge of vehicle axle spacing, determining which is particularly challenging, as it requires highly precise and sensitive sensors for reliable axle detection at regular traffic speeds. Studies have been conducted to overcome this challenge by using various sensors, or by estimating the axle configurations with uncertainty, however, the challenge remains.

Recently, a study was conducted by Mirzaei (2022) at the Centre for Structural Innovation and Monitoring Technologies (SIMTReC) to determine vehicle axle configuration using Geophones. It was found that geophones were able to reliably detect axle configurations with 95% confidence. This reference proposes a novel approach to improve axle detection and to measure GVW and axle loads. The results show that geophones provide a highly reliable way of detecting vehicle axles, and their signals also provide valuable insight into the calculation of the detected axle loads.

1.3 Goals and Objectives

The purpose of this research is to contribute to the field of Civionics by enhancing the precision of B-WIM systems, specifically focusing on the estimation of vehicle axle loads. This is to be achieved through the exploration of Geophones, an innovative sensor in the context of B-WIM. The goal of this study is to develop a BWIM system based on Geophones that can determine accurately not only GVW but also axle weights and their spacing while the vehicles travel on an instrumented bridge at regular speeds.

By achieving these goals and objectives, the research aims to advance the capabilities of BWIM systems, particularly in the accurate estimation of vehicle axle loads, paving the way for more efficient and automated bridge monitoring processes.

1.4 Thesis Layout

The thesis follows a step-by-step structure. Chapter 2, Literature Review, goes into the details of existing work done with a specific focus on axle detection and influence lines.

Chapter 3, Hardware Description, provides the details of bridge instrumentation, the sensors and their specifications, data acquisition devices and the electrical circuitry connecting everything together.

Chapter 4, Data analysis goes into the steps for how data is converted from raw voltages captured from sensors into vehicle characteristics.

Chapter 5, Results, validates the proposed methodology with field experiments, showing results for vehicle characteristics calculated by the proposed methodology against the real measured values.

Chapter 6, Discussion, goes through an example of one of the vehicles to demonstrate each step of the process and provide suggestions for future improvements.

Chapter 7, Conclusions, summarizes the results, states the limitations of the proposed methodology and provides suggestions for improvements.

2 LITERATURE REVIEW

2.1 Introduction

This chapter presents a review of the current literature concerning the advances in Bridge Weighing in Motion (BWIM) systems with a specific focus on axle detection and axle loads estimation. Bridges play a crucial role in transportation infrastructure, and ensuring their safety and structural integrity has been an important area of research for many decades. Over the years, researchers have explored various structural health monitoring techniques to monitor and maintain bridges effectively. Sensors such as strain gauges, accelerometers, load cells, and acoustic sensors have been used to analyze the dynamic responses of bridges under traffic loads. This multidisciplinary approach of Civionics has provided valuable insights into the complex behavior of bridges under different loading conditions.

Early methods for measuring vehicle loads include static weighing on stationary scales and Weighing-In-Motion (WIM) techniques. However, these methods come with their limitations. Static weighing requires trucks to stop at weighing stations, causing unnecessary delays in traffic flow. On the other hand, WIM techniques deploy sensor devices on the road surface, often resulting in poor durability and causing disruptions during installation and maintenance. To overcome these drawbacks, the B-WIM system has emerged as an innovative and non-disruptive alternative. This system utilizes instrumented bridges as weighing scales, enabling the measurement of vehicle weights during regular traffic flow. Despite advancements in sensor configurations and algorithms for B-WIM, one persistent challenge is the accurate detection of axle weights and their spacings.

A significant recent contribution to the field comes from a 2022 study conducted at the Centre for Structural Innovation and Monitoring Technologies (SIMTReC) by Maedeh Mirzaei.

The study proposes the use of Geophones for the reliable detection of axle configurations with an impressive 95% confidence level. Geophones, typically used to detect ground vibrations, demonstrated promise in accurately identifying axle configurations under varying traffic conditions. This breakthrough not only addresses the challenges highlighted in the literature but also opens new possibilities for improving axle detection methods in bridge weigh-in-motion systems.

2.2 Traditional B-WIM:

Bridge Weigh-in-Motion (B-WIM) technology originated in the early 1970s with pioneers Fred Moses and George Goble in the U.S. In the mid-1980s, Rob Peters applied B-WIM successfully to Australian bridges and later developed a simplified version for culverts.

Traditionally, a B-WIM system integrates two primary sensors: weighing sensors, which measure the overall bridge responses, and axle detectors, responsible for identifying axle spacing and vehicle speed. Initially, axle detectors were mounted on top of the road surface, raising concerns about durability due to direct contact with vehicles and potential disruptions to traffic flow during installation and maintenance.

To address these challenges, Nothing-On-Road (NOR) and Free-of-Axle Detector (FAD) emerged. Unlike traditional axle detectors positioned on the road surface, FAD sensors are installed beneath the bridge deck, improving durability, and eliminating traffic interference associated with on-road installations. Further details on each method are discussed below.

2.2.1 Moses

Moses introduced the concept of Bridge Weigh-in-Motion (BWIM) in 1979 as a study for the Federal Highway Administration (FHWA). He highlighted the potential advantage of longer contact time between the vehicle and the bridge compared to the pavement-based WIM devices. This extended contact time allows for more measurements, and dynamic effects can be minimized through a statistical smoothing algorithm.

The proposed BWIM system involved strain transducers installed on the bottom flanges of the girders near the middle of an exterior span. To determine axle spacing and velocity, axle detectors were required on the road, and tape switches were placed before the bridge. The study focused on a beam-slab bridge, and the bending moment M_k^m and predicted bending moment M_k^p at time step k for these bridges could be obtained using the influence line concept shown in Equation 1.

$$M_k^m = \sum_{i}^{N} ES_i\varepsilon_i \qquad\qquad M_k^p = \sum_{i}^{N} A_i I_i \left(k - \frac{D_i f}{v}\right) \qquad (1)$$

Where N is number of axles, E is the modulus of elasticity, and for the ith girder, S_i is the section modulus, ε_i is the measured strain, A_i is the weight, I_i is the influence ordinate at its current position, D_i is the distance between first axle and the ith axle, v is the vehicle speed, and f is the sampling frequency of the data acquisition system. Moses proposed using the least squares method to minimize the loss function between the predicted and measured responses of the bridge concerning axle weights. Through this approach, Moses was able to deduce that predictions of truck weights using an instrumented bridge span yielded promising results.

2.2.2 Rob Peters

In 1984, Australia marked a significant advancement in Bridge Weigh-in-Motion (B-WIM) technology with the development of the AXWAY system developed by R.J. Peters. The system aimed to determine axle and gross weights of passing trucks through instrumentation on a bridge. Peters utilized electrical resistance strain (ERS) gauges bonded to the deck reinforcement of the Maddington Bridge on the Beechboro Gosnells Highway in 1980 during its construction.

Despite its effectiveness, AXWAY was a manned system, incurring high costs for data collection. In response, Peters introduced a new unmanned system, CULWAY, in 1986. Described as a 'low cost/low power single lane system for unattended operation,' CULWAY weighed vehicle axles as they crossed over a culvert. The choice of a culvert over a bridge was driven by the quicker dampening of dynamic effects caused by vehicle-culvert interaction, facilitated by the surrounding soil.

Additionally, culvert-based WIM presented advantages such as the absence of abutments, reducing vehicle dynamic forces caused by even minor vertical misalignments between the approach roadway and the bridge deck. This innovation marked a notable progression in B-WIM technology.

2.3 Theoretical Influence Lines Calculations

Determining the influence line of a bridge is crucial for the accuracy of BWIM measurements. In the late 1990s, Dempsey and Žnidarič demonstrated that the transverse position of a vehicle in the lane affects the precision of calculated axle weights, especially for bridges with lower transverse stiffness (Dempsey et al. 1999; Žnidarič and Baumgärtner 1998). Many BWIM algorithms operate on the assumption that a load on the bridge induces a bending moment response proportionate to the product of the load's magnitude and the influence line (IL) ordinate at the load's position (Quilligan et al. 2002).

Practical bridge behavior may deviate from theoretical IL descriptions due to uncertainties in boundary conditions and material properties. Early BWIM systems, such as the CULWAY system (Peters et al. 1986), correlated peak values in measured responses but disregarded most response data. Addressing this, Žnidarič and Baumgärtner adjusted the theoretical IL to align better with measured truck data, using techniques such as smoothing peaks and adjusting boundary conditions (Žnidarič et al. 1998).

In 2003, McNulty and O'Brien proposed a manual point-by-point method for IL adjustment based on measured data, albeit dependent on operator skill (McNulty et al. 2003). A more automated approach by O'Brien et al. in 2006 involved calculating the IL from direct strain measurements. This method compared internal moments in the girders, determined by strain transducers, to external moments caused by the loads. The least squares method minimized the difference between the two curves, demonstrating effectiveness in improving IL determination accuracy in BWIM (O'Brien et al. 2006).

In 2020, Algohi et al. investigated the calculation of Gross Vehicle Weight (GVW) using the area method. The study specifically addressed the challenge of determining theoretical influence lines when trucks are in motion with variable velocities. Algohi et al. derived equations for both constant and variable velocities, confirming that dynamic response does not impact the area method. The study concluded that dynamic response does not affect the area method, because the dynamic effects cancel out when calculating the area under the curve (Algohi et al. 2020). This thesis assumes constant velocity on a medium span instrument bridge and uses the area method described by Algohi et al (2020).

2.4 Axle loads estimation

2.4.1 Reaction force method

Ojio and Yamada (2005) proposed a method which introduces a novel approach to calculate axle weights by utilizing the measured reaction force at the support of a bridge. This method relies on the influence line of the reaction force for a simply supported bridge. Notably, the influence line exhibits a distinct sharp edge at its onset, representing the maximum value of the reaction influence line as the unit load first applies to the bridge. This edge is assumed to be solely contributed by the axle load, allowing for the calculation of axle weights based on the edge's height.

The primary benefit of the Reaction Force Method is its simplicity and ease of use. An edge appears in the signal as each axle enters the bridge, making it suitable for axle detection. However, despite these advantages, the method faces practical issues. The method is restricted to bridges without skew, limiting its applicability in practical scenarios and it utilizes only the peak strain of the response, while ignoring the dynamic effects caused by axle forces, leading to errors in identifying axle weights.

2.4.2 Axle detection sensors development

Axle detection is a crucial aspect of BWIM systems as it enables the identification of vehicle axles, leading to the calculation of vehicle speed and axle spacing, which directly influences axle weight calculations. Traditional axle detection instruments include tape switches and pneumatic tubes. Moses (1979) highlighted that tape switches are easier to incorporate into the system, whereas pneumatic tubes require a pressure sensing device for axle passage signal generation.

Roadway axle detectors, such as pneumatic rubber tubes, tape switches, piezo, or optic-fiber sensors, were commonly used in early BWIM systems for monitoring traffic. Pneumatic tubes converted axle strikes into electronic signals (O’Brien et al. 2006). Permanent sensors, like those used in pavement WIM systems but of lower quality, were also employed (Znidaric et al. 2002). The Free-of-Axle Detector (FAD) concept, introduced by the WIM of axles and vehicles for Europe (WAVE) project (Kalin et al. 2006), removed axle detectors from the road surface, replacing them with additional strain transducers under the bridge deck. Efforts were made to demonstrate the applicability of FAD technology to bridges with orthotropic steel decks in 1998, showing promising accuracy (Dempsey et al. 1998). Znidaric expanded FAD to concrete slab bridges in 2002, concluding that FAD installation on thin slab spans less than 10 meters yields results like those obtained with axle detectors (Zindaric et al. 2002).

Some early FAD implementations could capture vehicle velocity but were unable to determine the number of axles or axle spacing (Ojio et al. 2000; Ojio et al. 2002). Optical sensors placed on the vertical members of a Warren truss bridge in 2000 captured vehicle velocity, providing GVW results within 10% of static weigh station weights (Ojio et al. 2002). In 2002, Ojio and Yamada instrumented reinforcing stringers of a plate girder bridge with a FAD BWIM system to monitor bridge fatigue, but this system did not measure axle loads (Ojio et al. 2002).

In a recent development, geophones have emerged as a novel type of sensor for axle detection, showcasing their potential in improving the accuracy of this crucial aspect in BWIM systems. A study conducted at the University of Manitoba by Mirzaei (2022), at SIMTReC, explored the use of geophones for determining vehicle axle configurations.

The study did not measure the axle loads but its findings revealed that geophones demonstrated a high level of reliability in detecting axle configurations, achieving a confidence level of 95% (Mirzaei, 2022). This represents a significant advancement in axle detection technology. Mirzaei's thesis highlights the successful application of geophones for axle detection. This innovative approach marks a notable contribution to the ongoing advancements in bridge monitoring and weigh-in-motion technologies. This thesis extends that study beyond axle detection, aiming to measure the vehicle GVW and individual axle loads.

2.5 Summary

In summary, estimation of axle loads has been a prominent topic in research. Pioneers such as Fred Moses and Rob Peters laid the foundation for B-WIM technology, addressing challenges and propelling innovations such as FAD systems. Theoretical influence line calculations showed refinements, with automated methods enhancing accuracy, as seen in the work of O’Brien et al. (2006). Additionally, the Reaction Force Method proposed by Ojio and Yamada provided a novel approach to axle load estimation. Notably, recent breakthroughs in axle detection, particularly the utilization of geophones, showcased promising results with a 95% confidence level, as evidenced in the 2022 study at SIMTReC. The current thesis extends this work, aiming to contribute to the advancement of the BWIM technology by exploring novel approaches to axle detection and load estimation, building on the momentum of recent innovations in the field of Civionics.

3 HARDWARE DESCRIPTION

3.1 Introduction

The methodology, outlined in Figure 1, details the data flow, starting with data acquisition from the instrumented bridge span through weighing and axle detection sensors. Subsequently, the Data Acquisition System (DAQ) samples this data, which can be stored locally or in the cloud for further analysis.

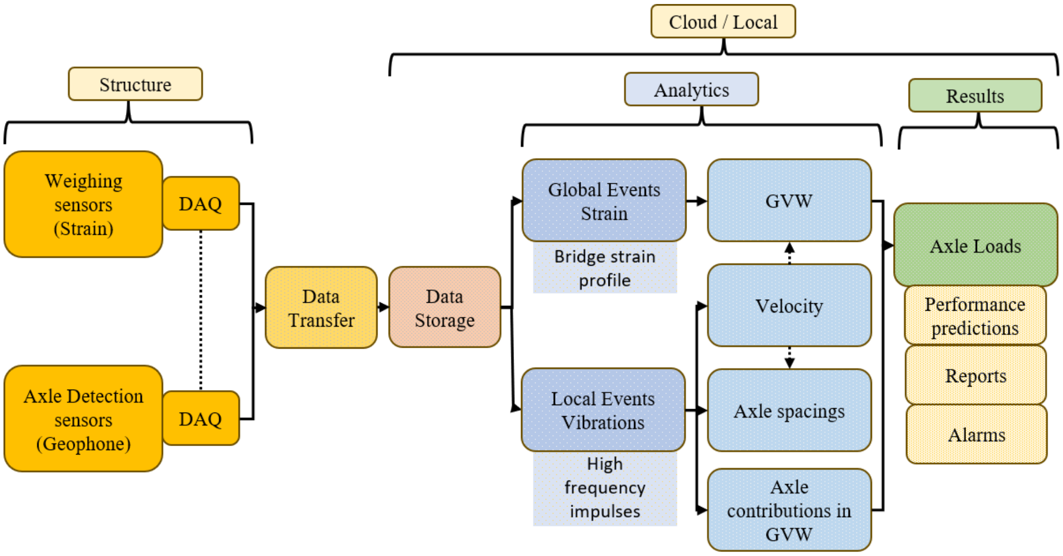

Figure 1 Overview of Research Methodology for BWIM

Once the data is stored, analysis is conducted to extract information from global events, such as the overall strain, and local events, such as the high-frequency vibrations caused by vehicle axles. This process yields the desired vehicle properties, including the GVW of the detected vehicle, its velocity, axle spacings, the contribution of each axle to the GVW, and ultimately, the individual axle loads. This information gives insight into the real traffic conditions of a bridge and may be used in performance predictions, reports, and alarms.

3.2 Bridge instrumentation

The South Perimeter Bridge (SPB) in Winnipeg, Canada, shown in Figure 2 was selected to be instrumented for field experiments. Figure 3 shows the side view of the bridge. It has four continuous and three simply supported spans. The overall superstructure is supported by eight steel girders. Span 1 was selected for instrumentation.

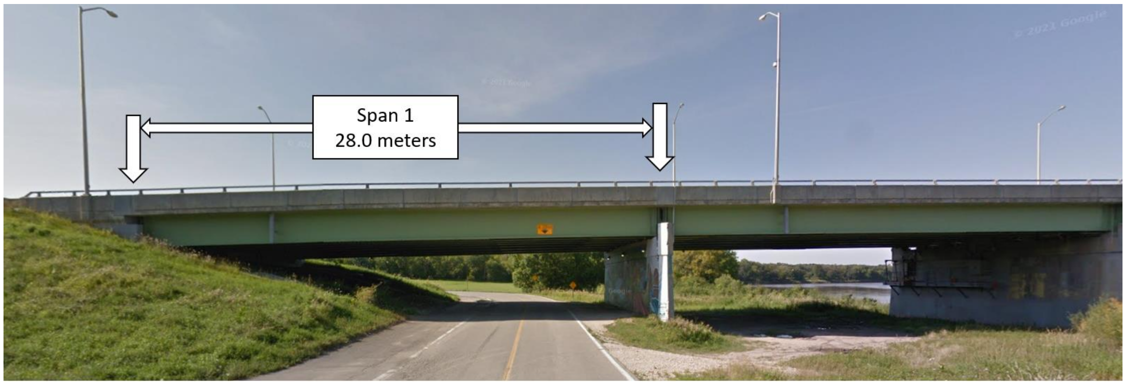

Figure 2 Partial image of SPB from google maps.

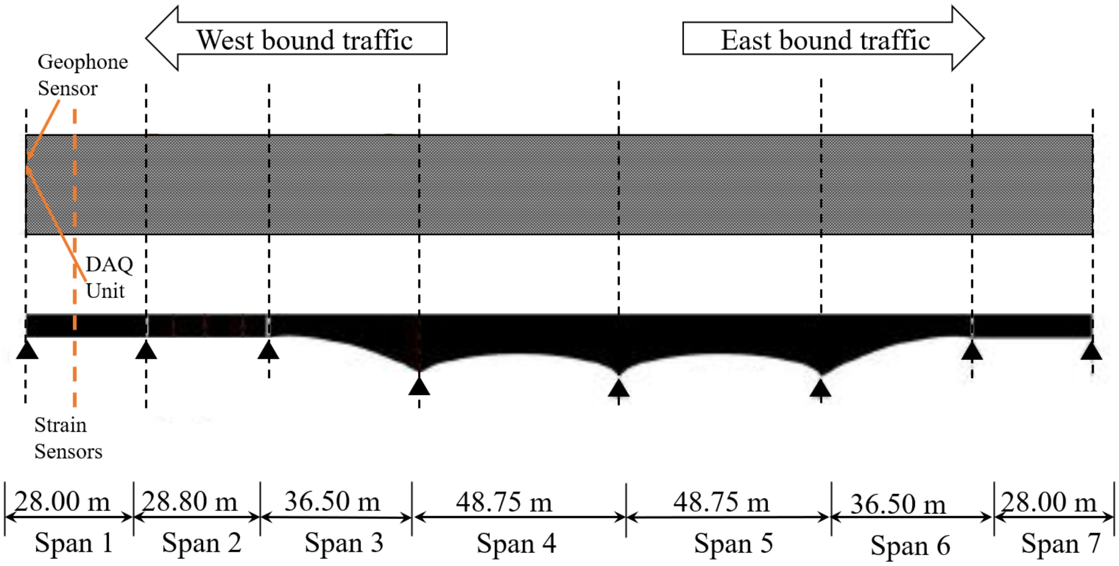

Figure 3 SPB Side View.

Figure 4 shows the cross section of instrumented bridge. Girders under eastbound lanes were selected to be instrumented. The selected span is supported by 4 girders. Figure 5 shows an illustration of the side view of the selected span. The bridge's instrumentation includes a geophone mounted on top of the bearing pad and 4 strain sensors placed 6.5 meters from the nearest girder support. The strain sensors were placed on each girder web 2 centimeters above the bottom flange.

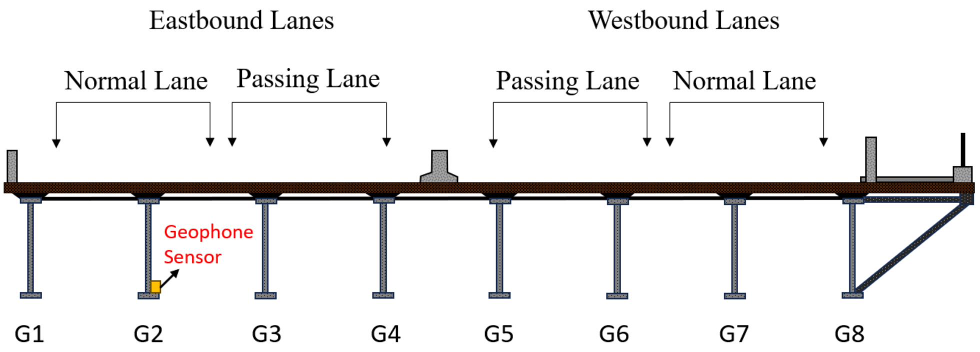

(a) cross-section near girder support

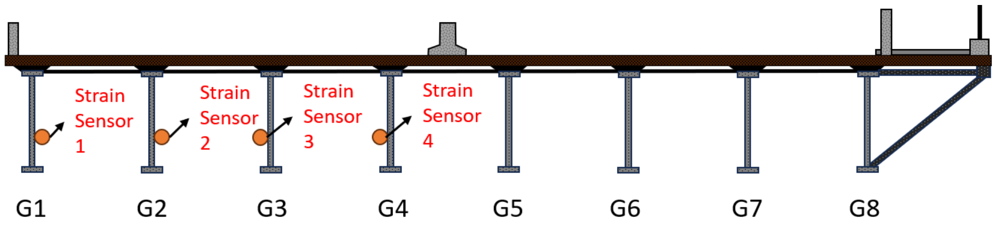

(b) cross-section at 6.5 m from girder support

Figure 4 Instrumented bridge cross-section view.

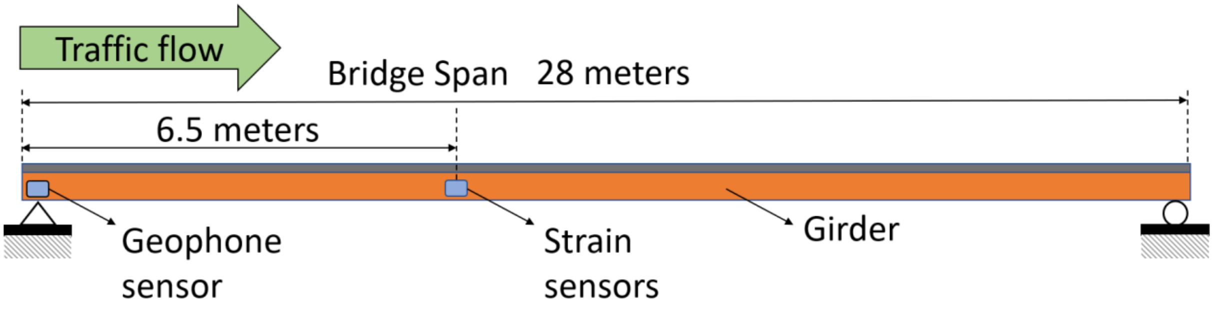

Figure 5 Side view illustration of sensors on instrumented span.

3.3 Weighing sensors

Strain sensors are typically made of a material that exhibits changes in electrical properties when subjected to strain, allowing it to convert mechanical deformation into a measurable electrical signal. Figure 6 shows the ST350 Strain Transducer that was used in this study. This sensor was chosen for its accurate and reliable readings.

Table 1 shows the important specifications for the sensor. Figure 7 shows the strain sensor mounted on the web of a steel girder.

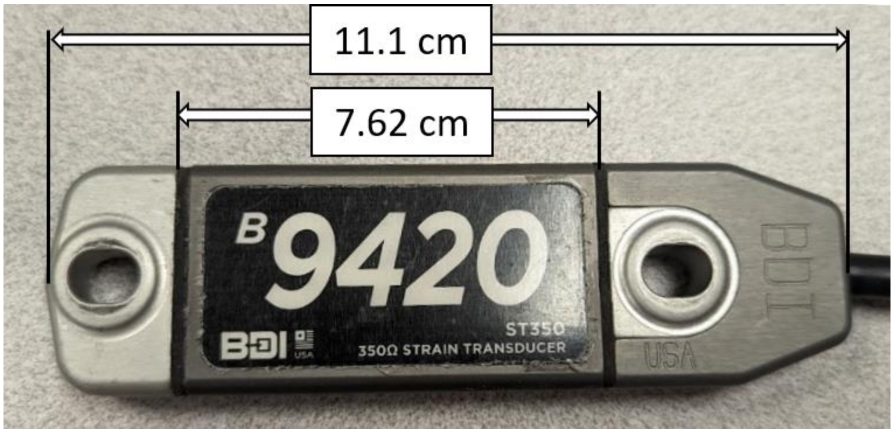

Figure 6 Photograph of Strain sensor

Table 1 ST350 Strain Transducer Specifications

Specification	**Value**
Circuit type	Full Wheatstone bridge
Strain Range	Calibrated to ± 2000 με
Sensitivity	500 $\mu\varepsilon/mV_{out}/V_{in}$
Effective gage length	7.62 cm
Size	11.1 cm × 0.32 cm × 1.27 cm

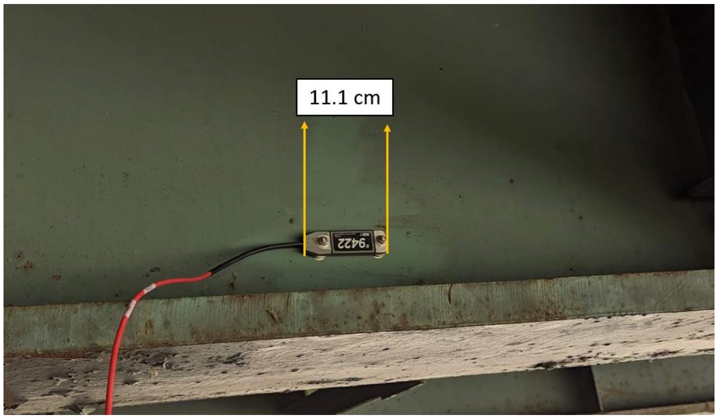

Figure 7 Photograph of one of the strain sensors mounted on the steel girder.

3.4 Axle detection sensors

A geophone is a sensor designed to detect ground vibrations by measuring the velocity. Unlike accelerometers, which require double integration for displacement, geophones need only a single integration. When a geophone experiences motion, the movement of the coil induces a current proportional to the velocity of the coil. The Results chapter demonstrates the performance of geophones for axle detection. Figure 8 shows the SG-5 geophone that was used in this study as axle detection sensor. Table 2 shows the important specifications for the sensor. Figure 9 shows the geophone sensor mounted on top of girder flange sitting right above the bearing pad.

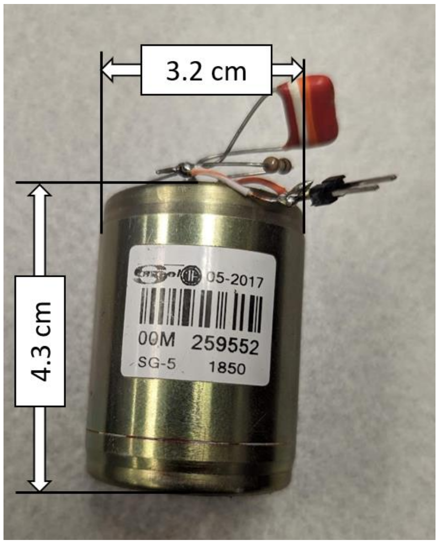

Figure 8 Photograph of the geophone sensor.

Table 2 SG-5 Geophone Specifications

Specification	Value
Natural Frequency	5 Hz
Strain Range	Calibrated to ± 2000 με
Sensitivity	80 V/m/s
Size (Length × Diameter)	4.3 cm × 3.2 cm

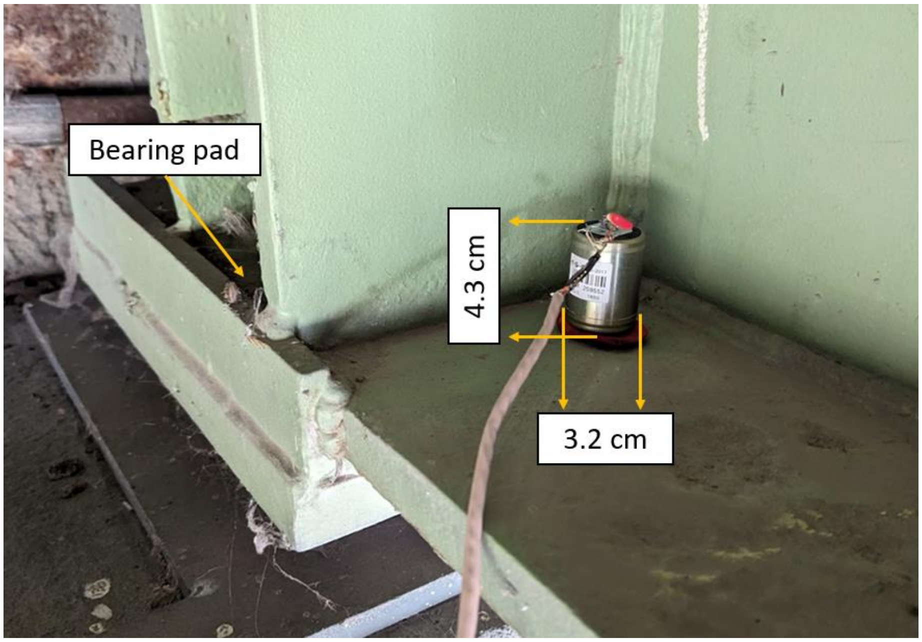

Figure 9 Photograph of geophone mounted on girder flange above the bearing pad.

3.5 Data Acquisition System (DAQ)

DAQ consists of devices that take electrical signals from sensors and convert them into digital data for analysis and storage. The device utilized for data acquisition is shown in Figure 10, and it was configured to sample data at 1 kHz across five channels. This sampling rate is chosen based on the geophone signal frequency for an axle event, which is approximately 50Hz. As discussed in "Axle loads calculation" section of the Data analysis chapter, the peak-to-peak magnitude of geophone signal is important for accurate measurements. With a 1 kHz sampling rate, the DAQ records around 20 readings for the geophone signal during a single axle event. This provides a finely sampled signal for further processing.

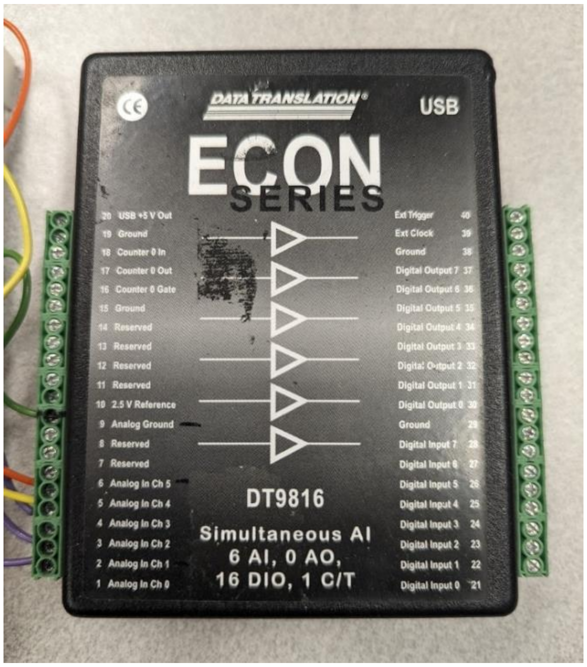

Figure 10 Photograph of the DAQ device

The DAQ device is accompanied by the "QuickDAQ" software system, installable on a computer to establish communication with the DAQ device. This software allows users to configure the DAQ, define sampling frequencies, set channels, and save the acquired data. The incoming data is stored locally in 5-minute chunks, and these data files are subsequently uploaded to cloud storage for further processing.

The choice of a 5-minute duration was made specifically for field experiments, ensuring manageable file sizes during the development of the methodology. With a 1 kHz sampling rate, each minute produces 4,020 kB of data, resulting in a 20,100 kB or approximately 20 MB file size for a 5-minute period. While larger file sizes may be used in the final BWIM product, the 20 MB threshold provides a balance between data volume and manageability in software environments like Matlab and Python, ensuring efficient processing without noticeable slowdowns.

3.6 Data transfer to cloud storage

Python scripts were developed to automate the process of uploading stored data to Google Cloud Storage, as depicted in Figure 11. The process involves sampling data from sensors through the DAQ, which is then stored on the local storage of the laptop. The Python script monitors the designated storage folder, identifying when a new file is saved. Once a new file is detected, the script initiates the upload of the file to Google Drive Cloud Storage. This cloud storage solution serves as a reliable backup mechanism and enhances data accessibility. Once the data is stored, it becomes available for further analysis, processing, and feature extraction, as elaborated further in the Data analysis section.

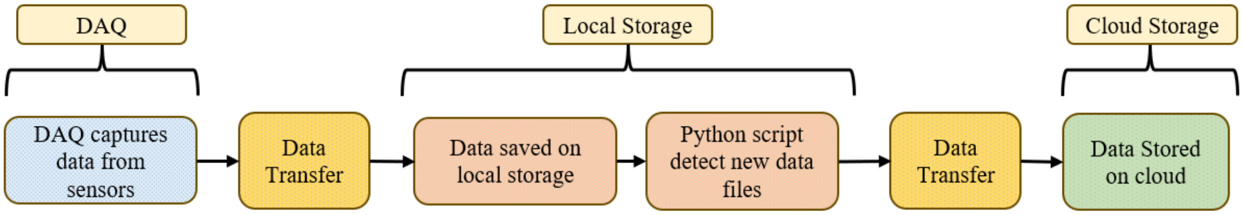

Figure 11 Illustration of data transfer from DAQ to Cloud via local storage

3.7 Electric circuit

3.7.1 Analog to Digital Converter (ADC)

The selected DAQ requires a digital signal. Given that the selected strain and geophone sensors produce analog signals, conversion into digital format is required. Furthermore, the magnitude of produced signals is typically very low and needs to be amplified with some gain. The INA126E ADC was used for this purpose. This ADC converts the signals from sensors into digital and amplifies it according to its circuit setup. This specific ADC only takes input from one sensor. So, 5 ADCs were used to convert signals from each of the 5 sensors. Figure 12 shows the circuit diagram for one of the sensors being connected to DAQ via ADC. Figure 13 and Figure 14 show photographs of this setup.

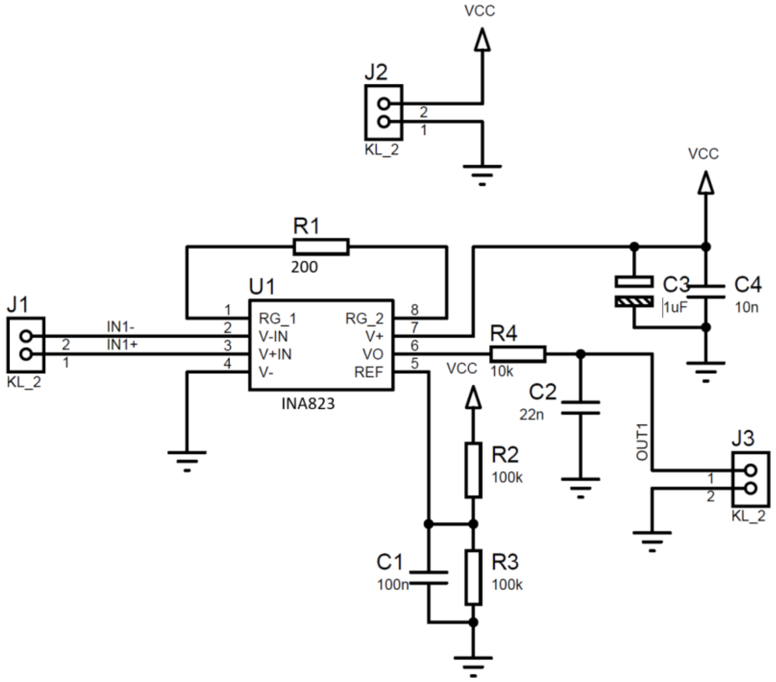

Figure 12 Circuit diagram for one sensor to ADC to DAQ wiring drawn by Zoran Trajkoski, University of Manitoba.

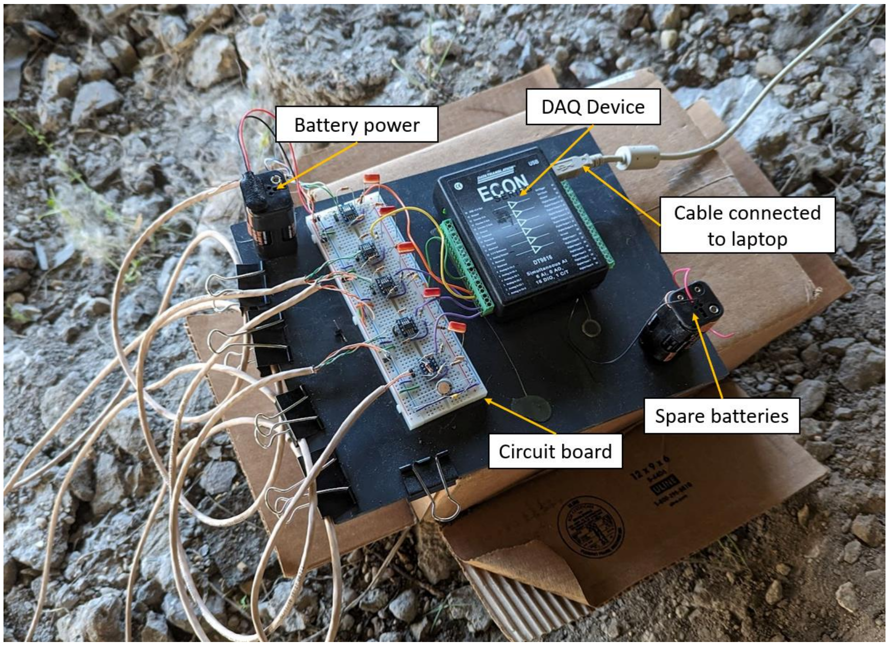

Figure 13 Photograph of the DAQ with sensors wired into the circuit board.

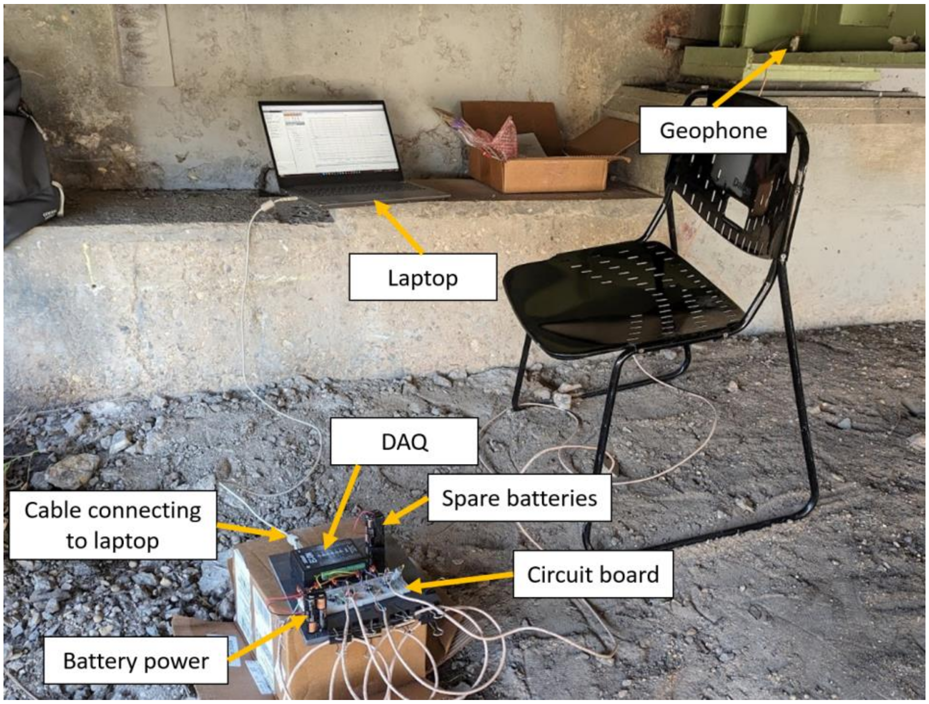

Figure 14 Photograph of the entire DAQ system connected to laptop for data collection.

4 DATA ANALYSIS

4.1 Introduction

This chapter provides the details of how raw data from sensors is processed to extract meaningful information. The data analysis workflow, illustrated in Figure 15, starts with the retrieval of sensor data. Raw data undergoes a pre-processing stage, where the unwanted noise is filtered out via moving average filters, and measured voltages are transformed into appropriate engineering units. During analysis, when a vehicle event is detected, a subset of this refined data is extracted containing the recorded strain profile of the vehicle and the vibrations caused by the impacts of axle wheels rolling onto the instrumented span.

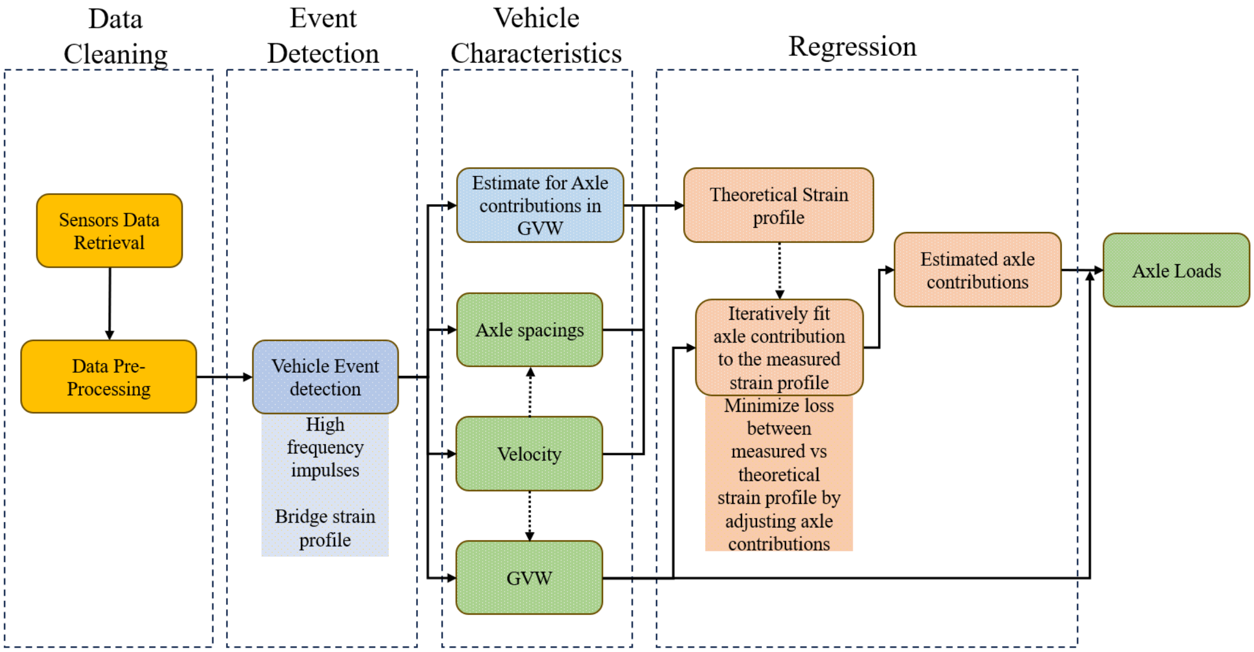

Figure 15 Illustration of the complete data analysis process.

From this refined subset, crucial information regarding the vehicle's velocity, axle configuration, and axle spacings is determined. An initial estimate for axle load contribution is derived from the Geophone signal, followed by regression analysis to fit the detected axle configuration's theoretical strain profile with the measured strain profile. Finally, the axle loads are determined by combining the GVW and the axle contributions from regression. Each step of this process is further explained in the following subsections.

4.2 Data Pre-Processing

Figure 16 shows the raw data as recorded by the DAQ software. The raw data consists of a total of five channels, one for Geophone and four for strain sensors, all sampled at 1 kHz.

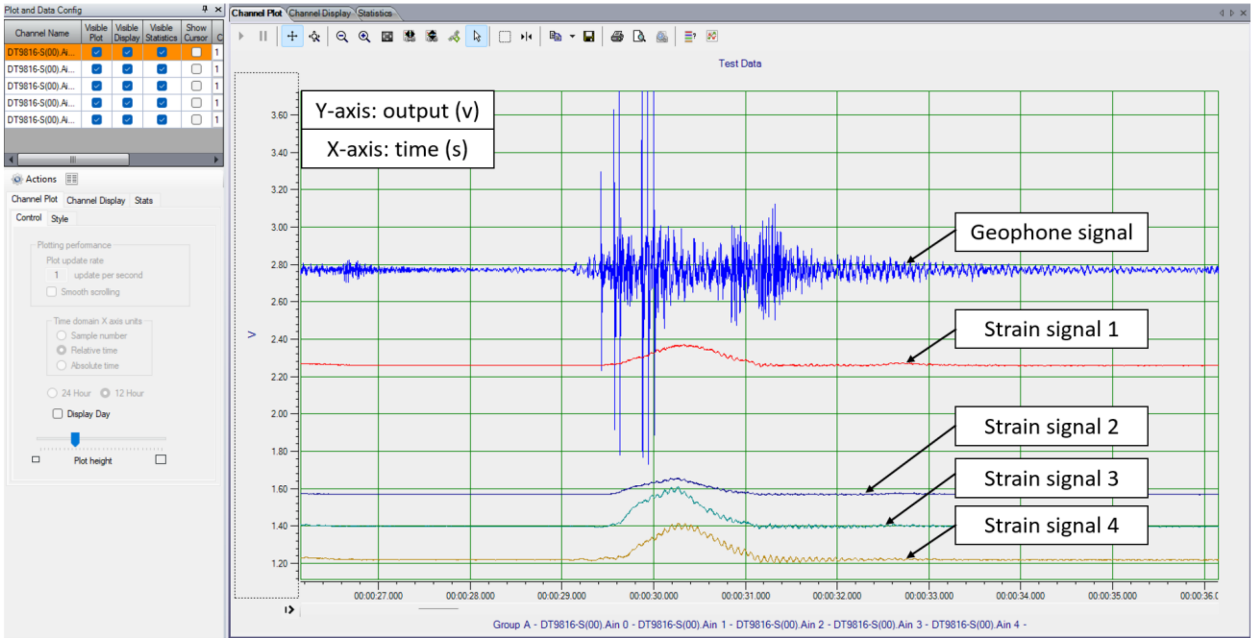
Plot and Data Config

Channel Name	Visible Plot	Visible Display	Visible Statistics	Show Cursor	C
DT9816-S(00).Ai...	☑	☑	☑	☐	1
DT9816-S(00).Ai...	☑	☑	☑	☐	1
DT9816-S(00).Ai...	☑	☑	☑	☐	1
DT9816-S(00).Ai...	☑	☑	☑	☐	1
DT9816-S(00).Ai...	☑	☑	☑	☐	1

Plotting performance
Plot update rate
1 update per second
☐ Smooth scrolling
Time domain X axis units
○ Sample number
● Relative time
○ Absolute time
○ 24 Hour ● 12 Hour
☐ Display Day

Group A - DT9816-S(00).Ain 0 - DT9816-S(00).Ain 1 - DT9816-S(00).Ain 2 - DT9816-S(00).Ain 3 - DT9816-S(00).Ain 4 -

Figure 16 Screenshot of QuickDAQ software capturing raw data.

4.2.1 Cleaning and Conversion

The sensors data need to be filtered for unwanted frequencies and converted from the electrical units i.e., volts to the respective mechanical units, such as "$\mu\varepsilon$" for strain sensors and "*mm/s*" for Geophone.

Strain data is first summed across all four channels to get the sum of strains across all girders. As shown in Table 1, the sensitivity of the strain sensors is 500 $\mu\varepsilon/mV_{out}/V_{in}$, with V_{in} of 6 Volts, and a gain of 200, the conversion becomes 5.7 $mV/\mu\varepsilon$. A moving average filter of window size 250 samples is applied to smooth out unwanted noise including vibration at the natural frequency of about 4 Hz.

As shown in Table 2, the sensitivity of geophone is 80 V/m/s. With excitation voltage of 6 V and gain of 18, the conversion becomes 0.6944 mV/mm/s. Finally, a moving average filter of window size 10 samples is applied to smooth out unwanted high frequency noise.

Figure 17 (a) shows the raw data as captured by the DAQ, focused on the signal for an example truck depicted in Figure 19. It is important to note that all data channel readings contain offsets that need to be removed for further processing. This was accomplished by subtracting the offset value for each channel from its respective readings. Figure 17 (b), shows the result of this step, with the offset for all signal channels set to zero. Afterwards, the strain signals are summed together giving the overall sum of strains as shown in Figure 17 (b). Finally, the resultant signals are converted from voltages into their respective engineering units by multiplying with the conversion factor as discussed in the above paragraphs. Figure 18 (a) shows the data converted form raw voltages into the engineering units. Finally, Figure 18 (b) shows the final result of data pre-processing after the moving average filters are applied.

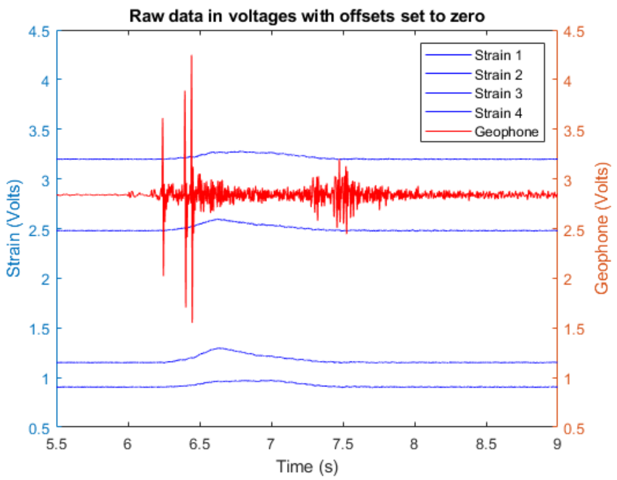

(a) Raw data in voltages

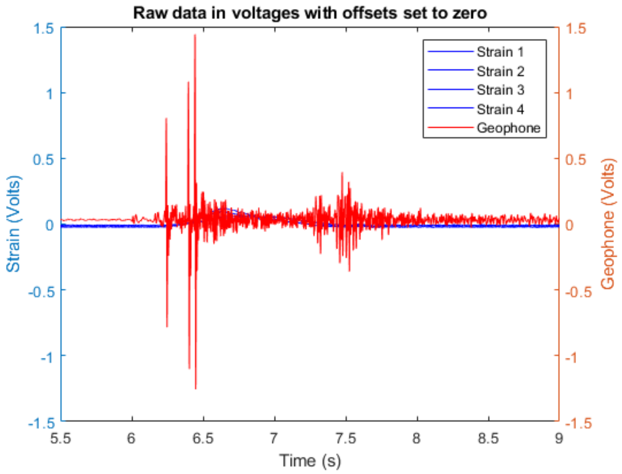

(b) Raw data in voltages with offsets removed

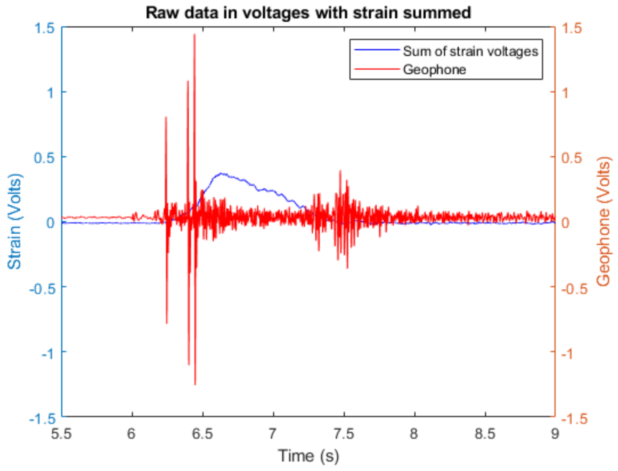

(c) Raw data in voltages with strain summed across channels.

Figure 17 Plots for sensors data captured in voltages

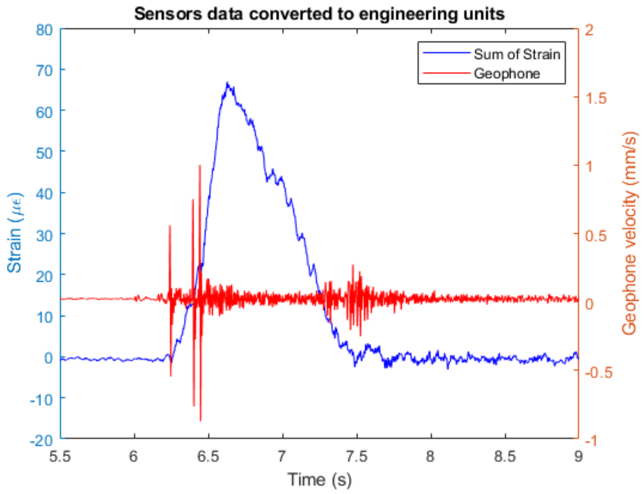

(a) Data converted into engineering units

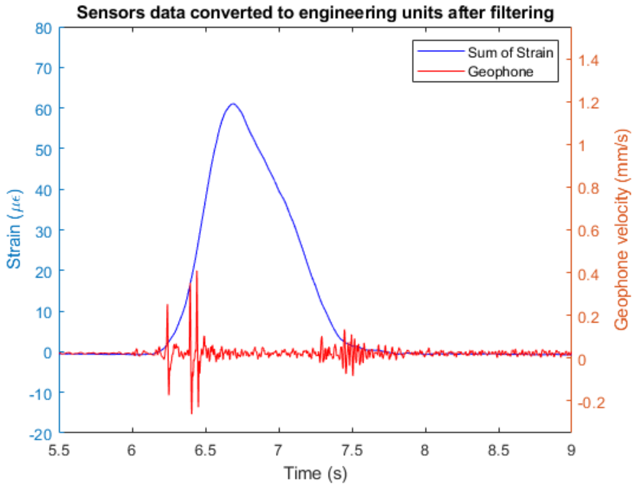

(b) Data in engineering units after filtering

Figure 18 Data plot for the result of pre-processing.

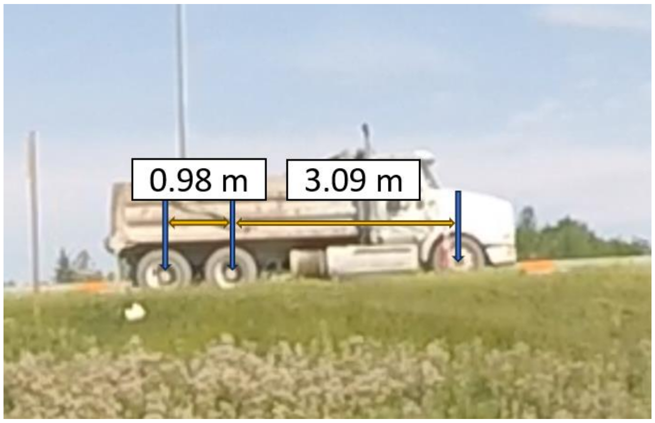

Figure 19 Photograph of the example truck used in methodology examples.

4.3 Velocity Calculation

The arrival time of each axle is detected by using the geophone signal peaks, as shown in Figure 20. When the vehicle axles travel the length of the span and roll off, they produce another high frequency event that is detected by the geophone placed at the start of the span. The shape of the departure signal is correlated to the shape of the arrival signal. However, since the departure signals have lower magnitude and are noisier, it is challenging to pinpoint an exact moment in time when the axle wheels roll off the span.

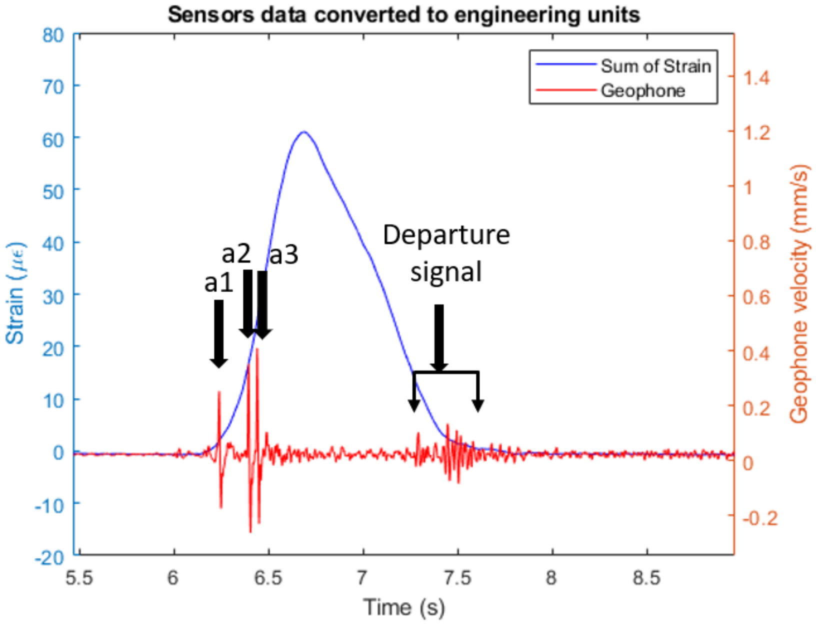

Figure 20 Plot of data showing peak in signal for each axle rolling onto the instrumented span.

To pinpoint the time for the departure of each axle, the signal arrival window is extracted as shown in Figure 21 and it is slid along the signal through time. Pearson correlation coefficient (PCC) is calculated for each data window using Equation (2), which gives a statistical metric for measuring the strength and direction of linear relationship between two variables. In this case, the window size to calculate PCC is 360 milliseconds, which is determined by the length of time from first axle arrival to last axle arrival. One potential impact of the chosen window size is that if a vehicle reduces velocity after entering the bridge span, the PCC window may not accurately align with the departure PCC window, introducing errors in velocity calculation. This was not observed in collected data, but it remains a potential issue in the proposed methodology.

$$\rho(A,B) = \frac{1}{N-1}\sum_{i=1}^{N}\left(\frac{A_i - \mu_A}{\sigma_A}\right)\left(\frac{B_i - \mu_B}{\sigma_B}\right) \qquad (2)$$

The time having maximum PCC value as shown in Figure 22 is determined to be the departure time window for the signal as shown in Figure 21.

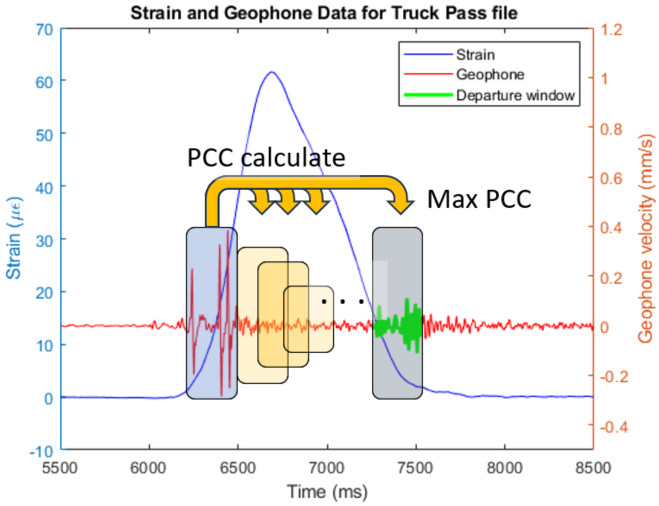

Figure 21 Plot of sensors signal with illustration of PCC calculation.

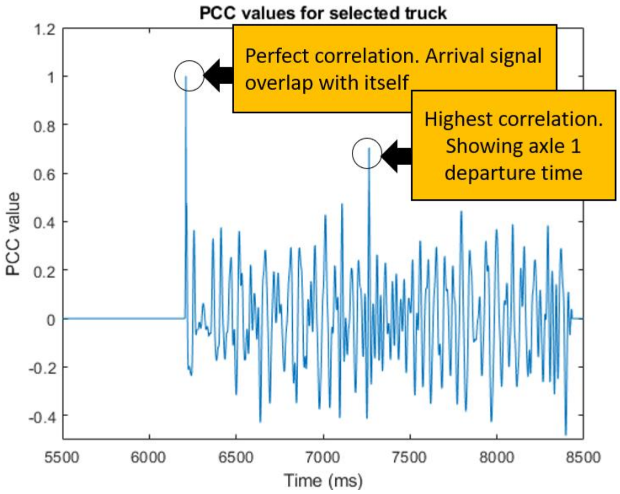

Figure 22 History plot of PCC values for arrival signal window slid across the example truck data with peak shown at exact arrival and exact departure time.

Figure 23 shows a representation of this process for a 3-axle vehicle. The annotated region is calculated to have the maximum PCC value of 0.7 and is selected. ΔT for the first axle is measured to be 1.1386 seconds. The length of the instrumented span is known to be 28 meters. Using this information, the velocity of the vehicle is calculated by dividing the span length over time, which was found to be 20.2 m/s.

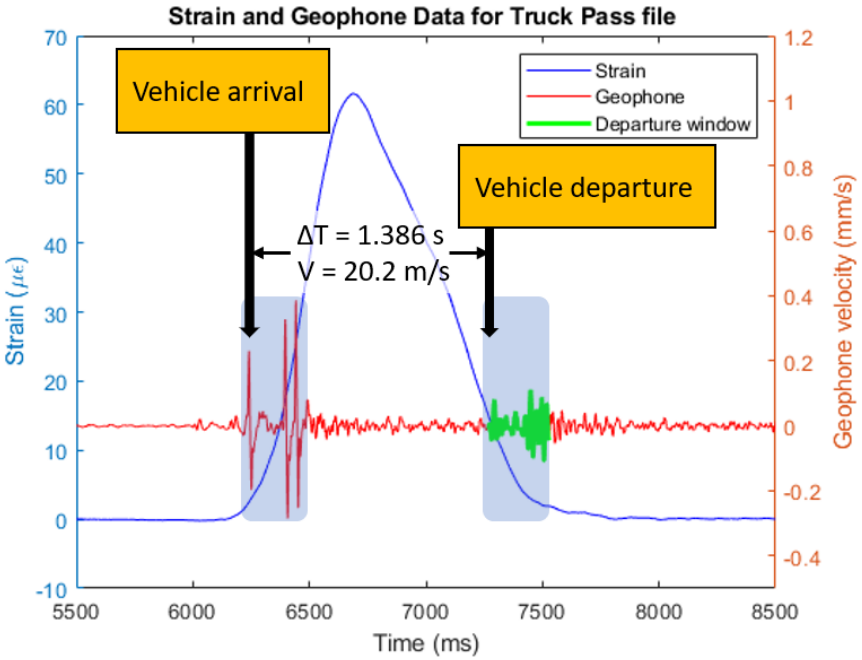

Figure 23 Plot showing velocity calculation via vehicle arrival and vehicle departure times for an example truck.

4.4 GVW Estimation

Using strain gauge data as shown in Figure 24, GVW is estimated using the area method equation as described by Algohi et al. 2020.

$$GVW = \left(\frac{2}{al(L-al)}\right).C\,.v\,.A_{V,t} \qquad (3)$$

Where L is the span length, aL is the distance of instrumented span from reference support, C is the constant calibration factor, V is the vehicle speed, $A_{V,t}$ is the area under strain-time curve.

Calculation of the calibration factor C needs to be measured by doing calibration runs with vehicles of known GVWs. In this study, the C value was determined to be 14.08. This process is further discussed in Calibration factor calculation. Figure 24 shows the measured signal for the vehicle shown in Figure 19. Equation (3) is used to estimate the GVW, which was found to be 122 kN.

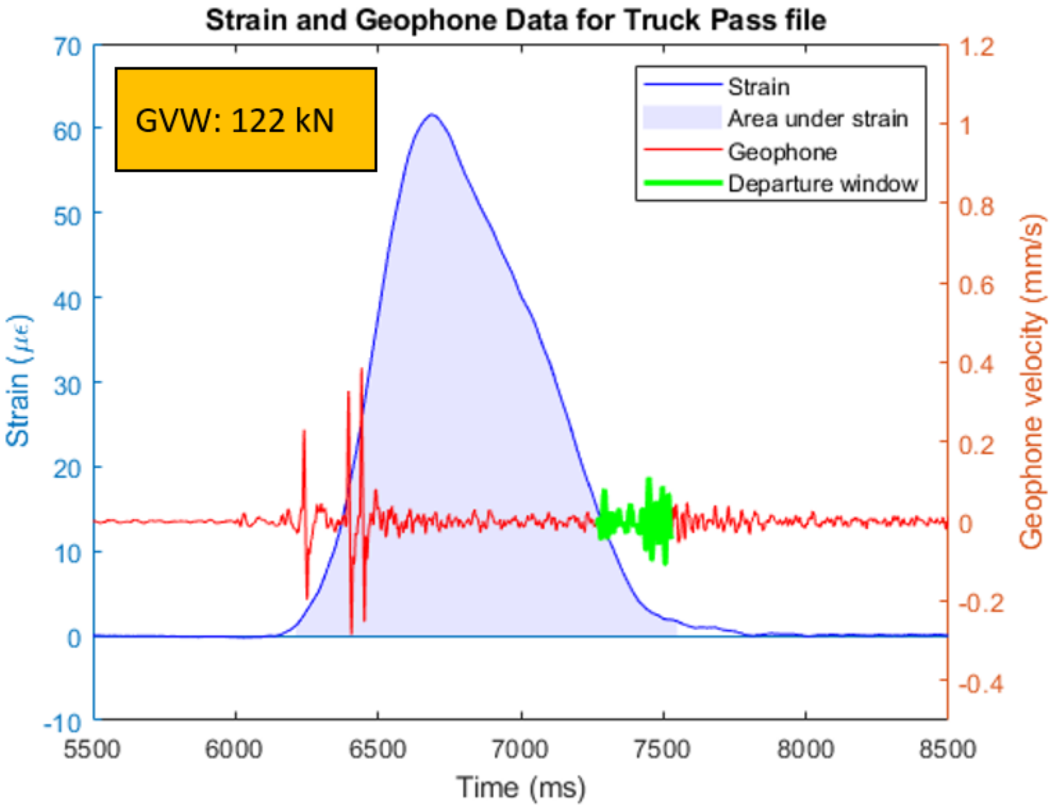

Figure 24 Plot showing the GVW calculation and area under the strain time curve for an example truck.

4.5 Axle Spacing Calculation

Using the vehicle velocity as measured in Figure 23 and the time for each axle peak as shown in Figure 25, the ΔT is measured for each axle peak with respect to the previous axle and multiplied with velocity. Table 3 shows the resulting axle spacings for the example vehicle shown in Figure 19.

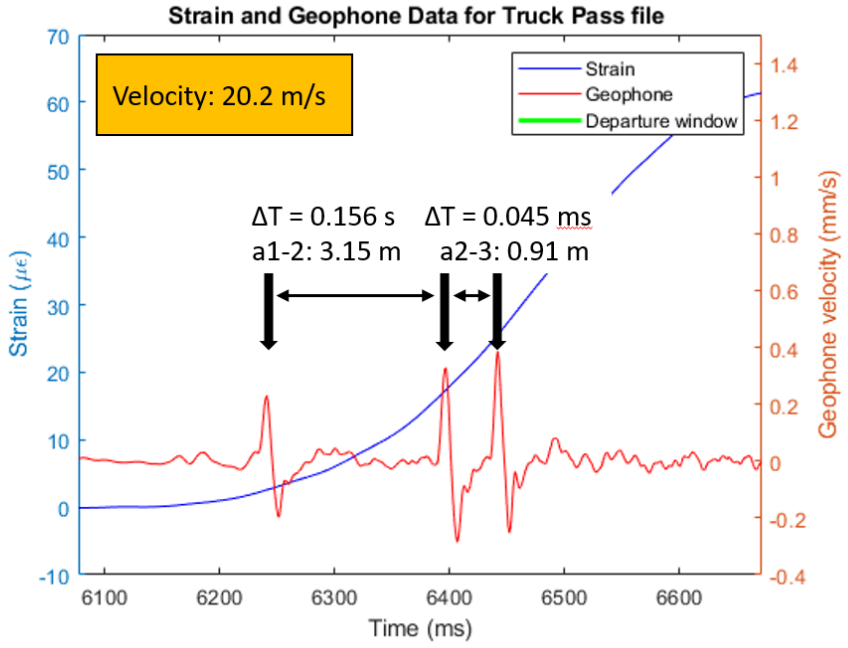

Figure 25 Plot showing axle spacings calculation using the velocity and the geophone peaks for arrival times for each axle.

Table 3 Table of calculated axle spacings for the example truck.

Axle	**Δ*T (s)***	**Axle spacing from data (m)**	**Reference Axle spacings (m)**
1-2	0.156	3.15	3.09
2-3	0.045	0.91	0.98

4.6 Theoretical Bridge response calculation for rolling axles.

4.6.1 Single axle

Consider a simply supported beam of span L with instrumented section at a distance *aL* from the left support, where *a* is a fraction of the span length. The influence line for the bending moments at the instrumented section for a single axle rolling over a beam, can be represented as shown in Figure 26.

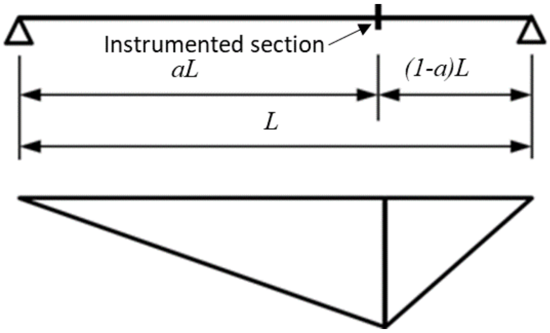

Figure 26 Influence line for single moving axle

Using a strain gauge at the instrumented section and a positive signal for strain, the ideal signal produced by passing a single axle along the length of the beam should have a magnitude of 0 at supports, and a maximum magnitude of 1 as the axle is on top of the sensor with a linear slope, as shown in Figure 27.

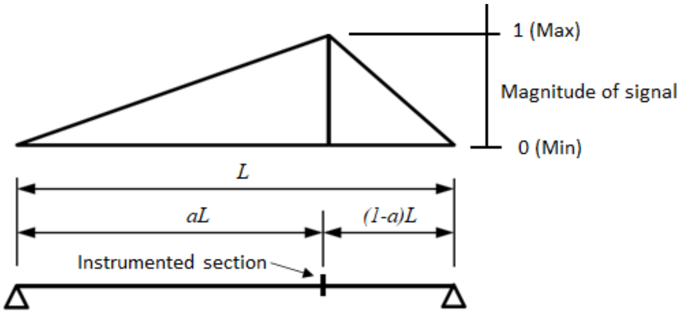

Figure 27 Ideal strain gauge signal for a single axle.

Mathematically, the response of an axle on a bridge deck at a time t can be calculated by Equation (4).

$$S_i(t) = I(x_i(t)) \cdot W_i \tag{4}$$

Where Si is the bridge response under the load of the ith axle, $I(x)$ is the influence line function of the bridge response relative to the load position, X_i and W_i are the location and the weight of the ith axle, respectively

4.6.2 Multiple axles

As more axles roll over the beam, the overall response of the beam will be the sum of the response of each axle, given by Equation (5).

$$S(t) = \sum_{i=1}^{N} S_i(t) \tag{5}$$

Where $S(t)$ is the overall response of bridge at time t and S_i is the bridge response under the load of the i^th axle.

Assuming a 4-axle truck with same load on each axle, and axle spacing of $v.(t_{ai} - t_{ai-1})$, where v is velocity of the truck, and t_{ai} is the geophone peak timestamp of i^th axle, the theoretical overall response of the bridge should be as shown in Figure 28 where blue line is the overall strain response, orange, green, red and purple are responses for each of the 4 axles: a1, a2, a3 and a4 respectively.

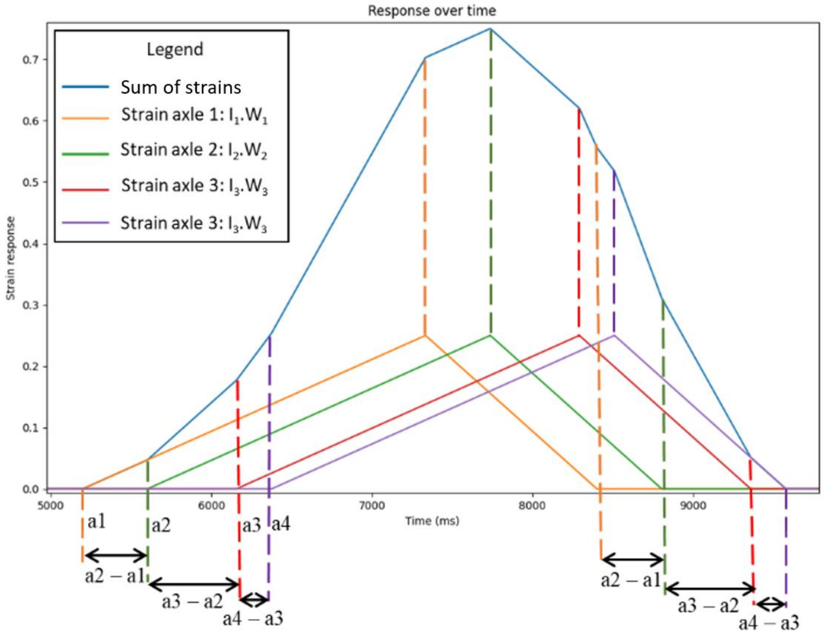

Figure 28 Plot of theoretical strain response for a 4-axle truck with equal weights across all axles

4.7 Axle loads calculation

Axle load calculation starts with an initial estimate of the axle load contribution for each axle in the GVW. Figure 29 shows the overall process for estimating the axle weights via regression. With the estimate for GVW, velocity, number of axles and axle spacing obtained from previous steps, regression can be used to fit axle weight parameters to minimize loss between the measured response of the bridge and the theoretical response by iteratively "fitting" the weight parameters until desired loss criteria is met. These weight parameters are normalized to provide the percentage contribution of each detected axle in the overall GVW estimate, arriving at estimates for each axle load.

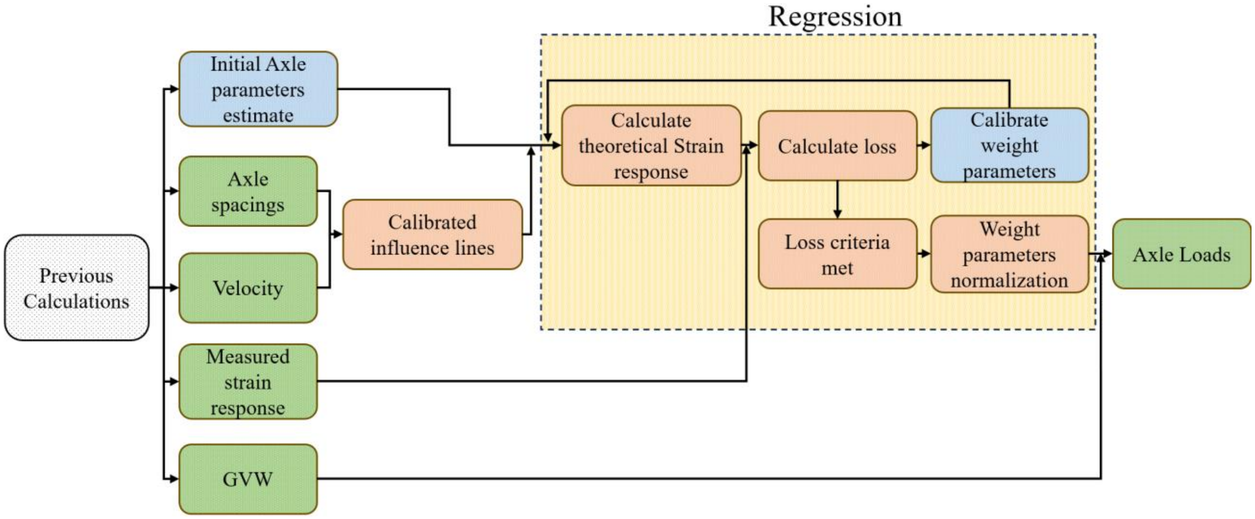

Figure 29 Illustration of the regression analysis step in data analysis.

4.7.1 Loss function

Mean squared error is used as the loss function given in Equation (6).

$$MSE = \frac{1}{N}\sum_{i=1}^{N}(S_i - S_i`)^2 \tag{6}$$

Where N is the number of readings, S_i is the measured bridge response at ith sample, and S_i` is the estimated bridge response at ith sample.

The estimated bridge response is calculated by Equation (7).

$$Si` = \sum_{i=1}^{a} I(x_i(t))\cdot W_i \tag{7}$$

Where a is the number of axles, $I(x)$ is the ordinate of influence line function of the bridge response relative to the load position, X_i and W_i are the location and the weight parameter of the ith axle, respectively and t is the moment in time. Finally, Equations (6) and (7) can be rewritten as Equation (8).

$$MSE = \frac{1}{N}\sum_{i=1}^{N}\left(S_i - \sum_{i=1}^{a} I(x_i(t))\cdot W_i\right)^2 \tag{8}$$

4.7.2 Normalized strain response

The shape and magnitude of the strain signal correspond to the load distribution per axle and the GVW respectively. Since GVW has already been estimated, the overall magnitude is no longer necessary, the measured strain response is normalized so that its magnitude lies between 0 and 1. This makes it so that the regression model can estimate weight parameters as a percentage contribution of the axle in the total GVW instead of an arbitrary parameter.

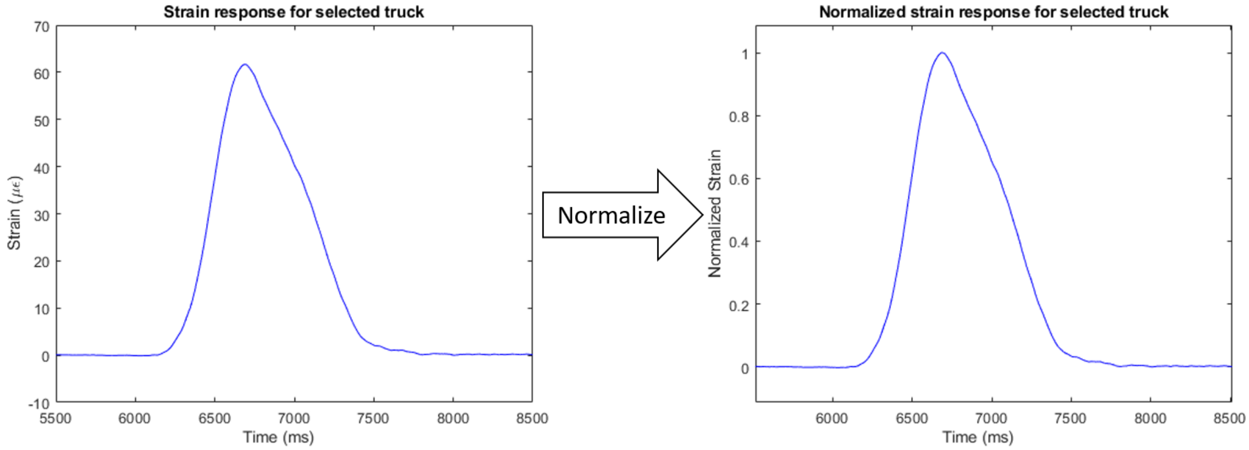

Figure 30 Figure showing strains before and after normalization.

4.7.3 Initial axle parameters estimate

The ratio of magnitude of geophone signal for each axle peak can be used as the initial axle weight parameters estimate. By taking the peak-to-peak geophone signal for each axle as shown in Figure 31, the initial parameters for ith axle are determined with Equation (9).

$$W_i = \frac{P_i}{\sum_{j=1}^{a} P_j} \tag{9}$$

Where a is the number of axles, W_i is the weight contribution of ith axle, and P_i is the peak-to-peak magnitude of geophone signal for ith axle. Table 4 shows the calculated magnitudes.

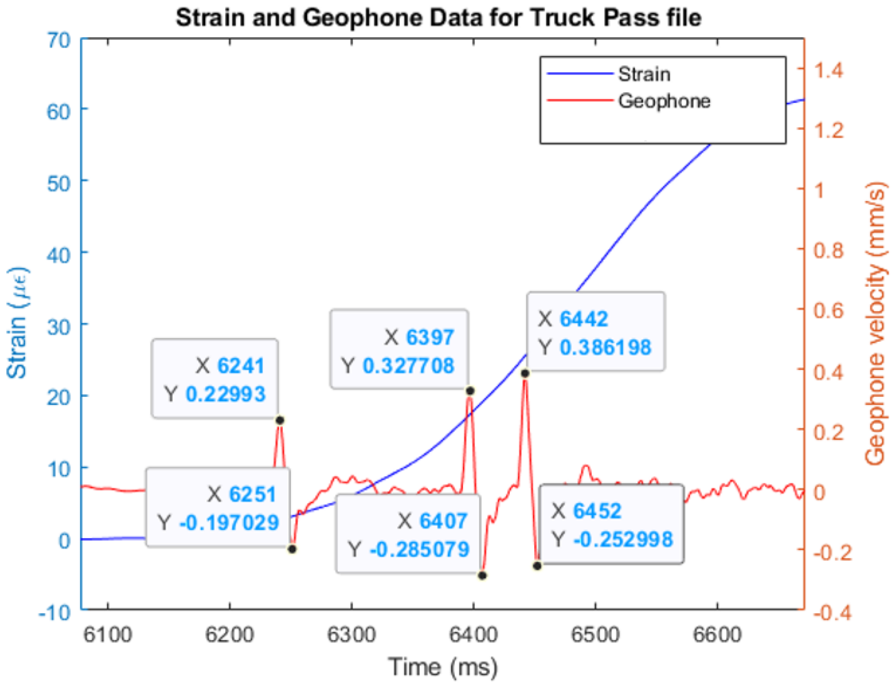

Figure 31 Plot showing the peak-to-peak signal used in initial axle load estimates

Table 4 Table of the peak-to-peak values converted into contribution percentages.

Axle	Peak to Peak response from geophone (mm/s)	Percentage Contribution
1	0.42696	25.43 %
2	0.612787	36.50 %
3	0.639196	38.07 %

4.7.4 Gradient descent

Weight parameters are iteratively updated for each axle to minimize loss using Equation (10).

$$\frac{\partial l}{\partial W_i} = -\frac{2}{N}\sum_{i=1}^{N}\left(S_i - \sum_{j=1}^{a} I_{ij}.W_j\right).(W_i) \tag{10}$$

Where N is the number of readings, S_i is the measured bridge response at ith sample, a is the number of axles, I is the ordinate of influence line function of the bridge response for ith sample and jth axle and W_i is weight parameter of the ith axle, respectively.

4.7.5 Loss criteria:

Loss criteria defines the condition to stop updating weights. It was found that weight parameters are typically calibrated within 8-10 iterations with worst case scenario being 20 iterations. Gradient descent in Figure 32 show an example of the process. Figure 32 (a) shows the theoretical strains overlaid on measured strains using weights shown in Figure 32 (b). According to the strain profile, the first axle magnitude was underestimated by the geophone. With further iterations, this was corrected as shown in Figures 32 (c) and (d). Figure 32 (e) shows the history of the weights updated over each iteration and Figure 32 (f) shows the calculated loss history over iterations.

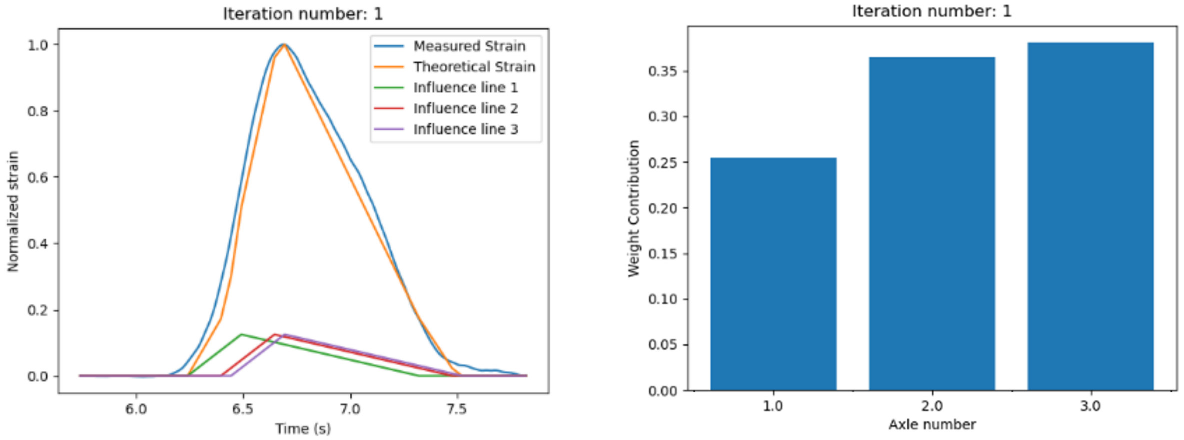

(a) Theoretical vs Measured strain at iteration 1. *(b) Weights at iteration 1.*

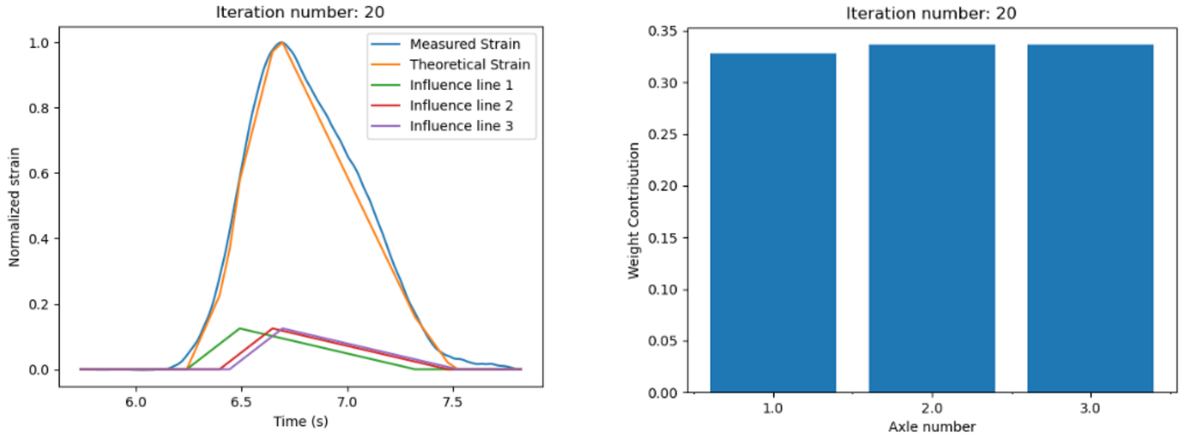

(c) Theoretical vs Measured strain at iteration 20. *(d) Weights at iteration 20.*

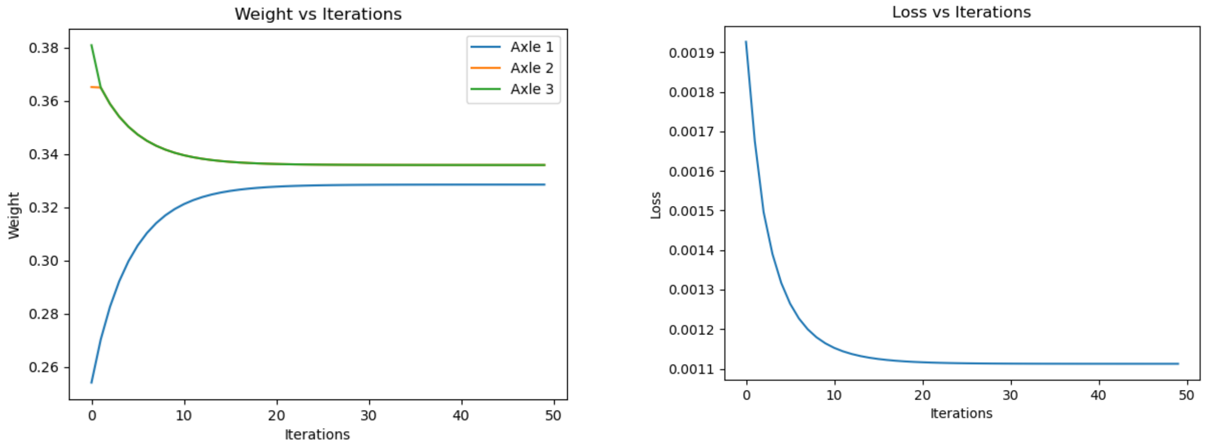

(e) Weight update history over 50 iterations. *(f) Loss update history over 50 iterations.*

Figure 32 Plots of gradient descent weight updates over iterations

4.7.6 Axle Loads

Finally, the calibrated weight parameters can be multiplied with the GVW to get the axle weights for each detected axle. Figure 33 shows the final reconstructed response over time.

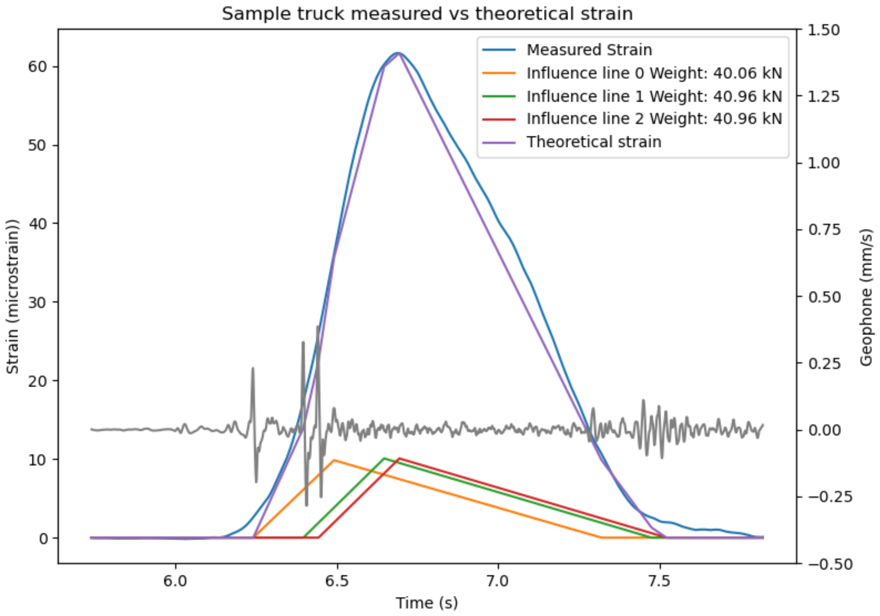

Figure 33 Result the Theoretical vs measured strain at the end of regression process.

Table 5 Result of calculated axle loads for an example truck with GVW of 122 kN.

Axle	Axle load (kN)	Contribution %
1	40	32.8 %
2	41	33.6 %
3	41	33.6 %

5 RESULTS

This chapter presents an assessment of the conducted field experiments and the performance metrics of the results.

5.1 Introduction

Field experiments were conducted on the SPB. Calibration experiments involved loading up a truck and measuring its axle loads at a stationary weighing station. This truck was driven over the instrumented bridge a total of twelve times. Data and video images were recorded for 5 minutes each time the test truck made a pass.

Figure 34 shows the overall setup of the field experiments. A video camera was set up near the entrance of the bridge to record passing vehicles and to validate axle measurements. Three traffic posts were placed with known distances to determine vehicle velocities.

There were three technicians. One technician was stationed at the instrumented bridge span recording and monitoring the data, one was stationed at the camera recording video feed of the side profiles of passing trucks and one was sitting with the driver in the truck. Coordination was done via phone. Data for each calibration run was recorded and stored for later processing.

It is important to note that the camera cone of vision does not cover the instrumented bridge span. This is because the landscape of the test site made it impossible to position the camera in a way that covers the instrumented span while still recording the axles of passing trucks.

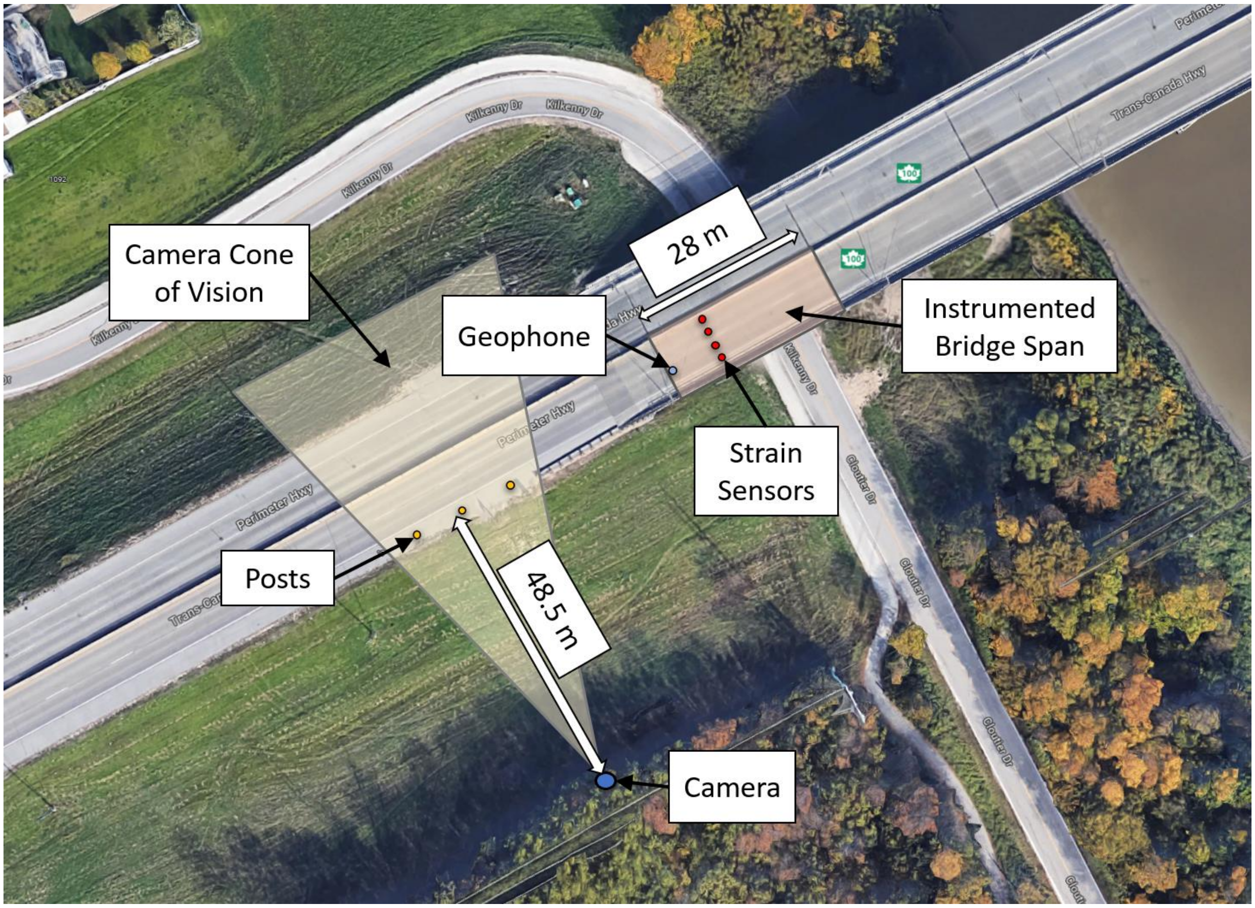

Figure 34 Satellite view of the field experiment set up. Image taken from google maps.

5.2 Field Experiments

The aim of field experiments was to collect bridge response data for a vehicle of known axle loads to determine the C Factor as discussed in GVW Estimation and to validate the results the developed methodology.

The field experiments were conducted twice, with the primary difference between them being the GVW and Axle loads of the calibration truck. One takeaway from the first experiment was the determination of the minimum axle loads required for grouped axles to be reliably detected by the geophone sensor. This was then validated with the second experiment.

5.2.1 Field experiment 1

Figure 35 shows a three-axle calibration truck, and its real axle loads as measured by the static weighing scale. Results for the seven calibration passes are further discussed in Calibration factor calculation. To validate the axle configuration detection, data was collected for 72 other trucks. Video feed was matched with the measured signals and the results for velocity comparisons are further discussed in Data velocity.

Figure 35 Image of the calibration truck for field experiment 1.

5.2.2 Field experiment 2

Field experiment 1 demonstrated the limitation of sensitivity of the geophone sensor for grouped axles. It was found that if axles are in a group of two or more, they each need to weigh at least greater than 40 kN to be reliably detected by the geophone. This is an important limitation of the sensor, which implies that empty tandem axle groups are not detected reliably. This necessitated field experiment 2 to validate the axle loads estimation along with these new findings.

Figure 36 shows the three-axle calibration truck and its real axle loads as measured by the static weighing scale. The calibration truck was the same as experiment 1. The only difference here was that this time it was loaded with heavier loads to meet the minimum load requirement for consistent detection as observed in experiment 1. In experiment 2, all three axles were detected consistently in all five runs. Further details about the analysis are discussed in the following subsections.

Figure 36 Image of the calibration truck for field experiment 2.

5.3 Video velocity calculations

5.3.1 Video Calculation

To validate the geophone velocity estimation, traffic posts were placed with known distances as shown in Figure 37. Timestamps were recorded when the center of an axle coincided with the center of a post, specifically for the first axle against each post. By calculating the time difference between the timestamps of post 1 vs. 2 and post 2 vs. 3, two velocity estimates based on the video footage were derived. Figure 39 shows the frame timestamps as taken for one of the calibration runs. Furthermore, it is important to note that the video was recorded at 60 frames per second with each successive frame having a time difference of approximately 17ms.

Figure 37 Image of the calibration truck and posts as visible from the field experiment camera.

Table 6 shows the comparison between the calculations from both sources. This method was followed for 72 trucks in the dataset. The average difference was only 0.012 m/s, with an R2 value of 0.98, showing the reliability of this method. An average of both velocities was used as a performance metric as discussed further in Data velocity.

Table 6 Results of video velocity comparison as calculated for Post 1 vs 2 and Post 2 vs 3.

Average difference	0.012 m/s
Sample size	72
R^2 value	0.98
Standard deviation	0.27

Figure 38 shows the plot of velocity comparison between different posts in the video. A clear linear correlation can be observed, giving confidence in using this method as a metric for comparison with the geophone data velocity.

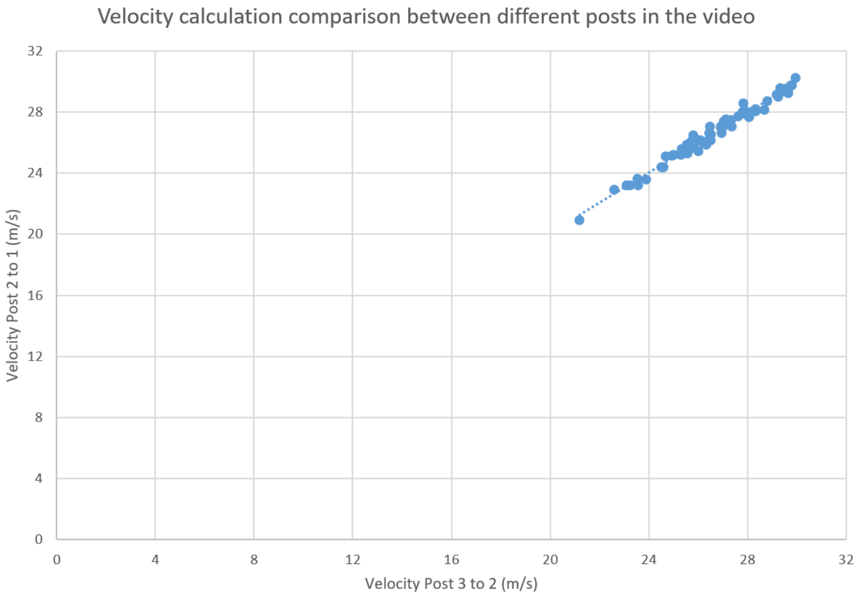

Figure 38 Video velocity plot for post 2 to 1 and 3 to 2

Figure 39 shows screenshots of the video footage with the timestamp of the test truck intersecting with each of the posts. A software “Avidemux” was used, selected for its ability to navigate frame by frame and view the timestamps in milliseconds. Unlike many other video players that default to displaying time in seconds, this software provides timestamps with precision down to milliseconds for each frame in the video. This precision is essential for accurate velocity calculations from video footage, which is why this software was used.

Figure 39 Screenshots of the calibration truck axle 1 overlapping with posts 1, 2 and 3.

5.3.2 Video Velocity Validation

To validate the results of velocity calculation from video, second and third axle times were noted in a similar manner for the 7 calibration runs and the measured velocity was used to calculate the axle spacings for the calibration truck. Table 7 shows the comparison of axle spacings calculated from the video verses the real measurements. The error and standard deviation prove that video can be used as a benchmark to assess velocity estimations from geophone data.

Table 7 Error in results for axle spacings using velocity and timestamps from video.

Axles 1-2	**Error range**	-1.93%, 1.25%
	Average error	-0.46%
	Maximum Absolute Error value	0.10 m
	STD Deviation	0.067
Axles 2-3	**Error range**	-1.76, 3.1%
	Average error	0.51%
	Maximum Absolute Error value	0.04 m
	STD Deviation	0.023

5.4 Data velocity

The velocity calculated from the geophone data was validated by using the velocity calculated from the videos. Table 8 shows the performance metrics of this comparison for the test truck, and Figure 40 shows the comparison for 64 trucks and Figure 41 shows the probability distribution in velocity error.. There is a clear linear correlation between the velocities. The error in velocity measurements was in the range of -5% to 3.8%, with 95% confidence interval of -0.4% and 0.54% and R^2 value of 0.95%.

Table 8 Comparison of test truck velocity from video footage vs geophone data

Error range	**-5% to +3.8%**
Average error	0.071%
Sample size	64
95% CI average error	(-0.4%, 0.54%)
Error Standard deviation	1.9%
95% CI standard deviation	(1.6%, 2.3%)
R^2 value	0.95

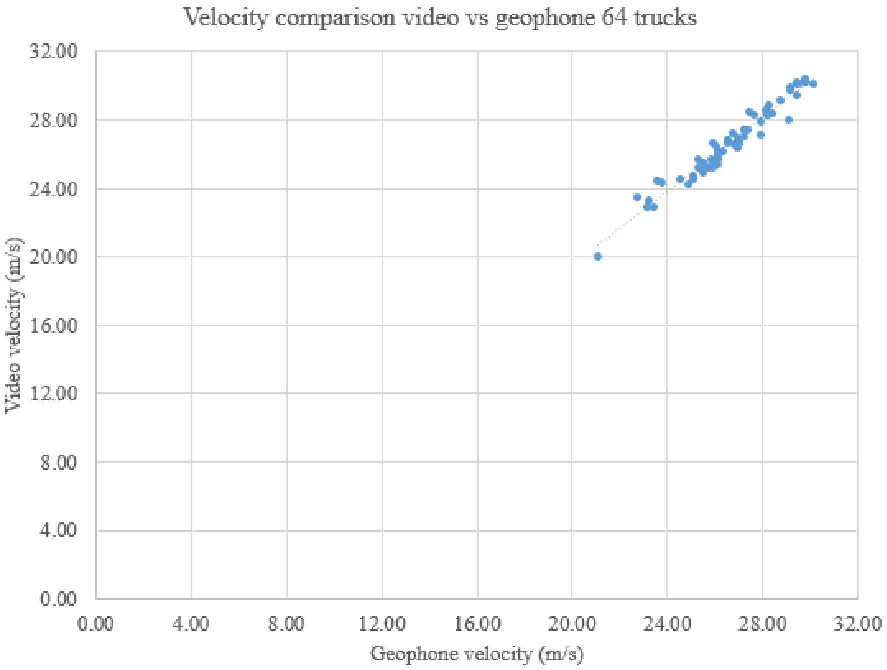

Figure 40 Plot of comparison of velocities from video vs geophone for 64 trucks.

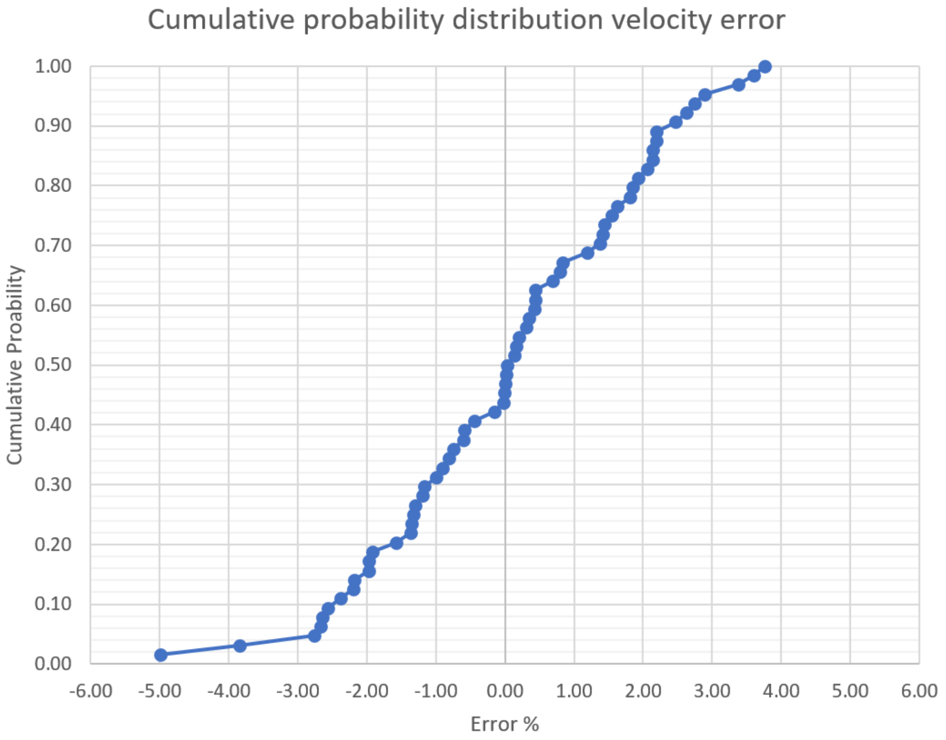

Figure 41 Plot of cumulative probability distribution in velocity error in geophone data velocity against video footage velocity.

5.5 Calibration factor calculation

To accurately determine the C factor, it is required that the GVW should be known. When there is another vehicle traveling along the instrumented span simultaneously with the test truck, then the actual load on the bridge becomes unknown. Despite the attempts to get clean signals for just the test truck without other vehicles on the span, some runs still had other vehicles. Those runs were discarded in the calculation of C factor. Among the twelve calibration runs, six clean runs, highlighted green in Table 9 were chosen to calculate the C factor. Details for each chosen run is shown in Table 9. Table 10 shows the summary of C calculation. The average value was calculated to be 14.08, with a standard deviation of 0.39 and a variance of 0.16.

Table 9 C Factor calculation table

Experiment 1		
Run #	**C value**	**Note**
1	14.34	Empty bridge
2	13.67	Empty bridge
3	10.7	Large truck opposite traffic
4	13.33	Small truck in passing lane
5	16.71	Small truck in passing lane
6	17.32	Small truck in passing lane
7	13.8	Empty Bridge
Experiment 2		
1	8.8	Large truck opposite traffic
2	14	Empty bridge
3	14.74	Empty bridge
4	13.93	Empty bridge
5	12.57	Small truck in passing lane

Table 10 Summary of C factor calculation

AVERAGE C	14.08
STD DEV	0.39
Variance	0.16

5.6 GVW

GVW was calculated as described in GVW Estimation. It was validated against the known GVWs from experiment 1 and 2. The six clean runs as described in Calibration factor calculation were selected for validation performance. Table 11 shows the results from six selected runs, with maximum error magnitude being 7 kN and error being in the range of -4.6% to +3.2%.

Table 11 Results for GVW calculations in experiments 1 and 2.

<table>
<tr><th colspan="4">Experiment 1</th></tr>
<tr><th>Real GVW (kN)</th><th>Calculated GVW (kN)</th><th>Absolute error (kN)</th><th>Error %</th></tr>
<tr><td rowspan="3">125</td><td>123</td><td>2</td><td>-1.6</td></tr>
<tr><td>129</td><td>4</td><td>3.2</td></tr>
<tr><td>128</td><td>3</td><td>2.4</td></tr>
<tr><th colspan="4">Experiment 2</th></tr>
<tr><td rowspan="3">154</td><td>155</td><td>1</td><td>0.65</td></tr>
<tr><td>147</td><td>7</td><td>-4.55</td></tr>
<tr><td>156</td><td>2</td><td>1.30</td></tr>
</table>

Due to known GVW sample size being small, t-distribution was used in calculating the confidence interval. Table 12 shows the performance metrics of GVW calculations, and Figure 42 shows the cumulative probability distribution for the measured errors in GVW. Error is in the range of -4.6% to +3.2%, with 95% confidence interval being -2.7% to 3.2% for a sample size of 6 runs with known GVWs.

Table 12 Performance metrics of GVW calculation

Error range	**-4.6% to +3.2%**
Average error	0.23%
Sample size	6
95% CI average error	(-2.7%, 3.2%)
Error Standard deviation	2.86%
95% CI standard deviation	(1.8%, 7%)

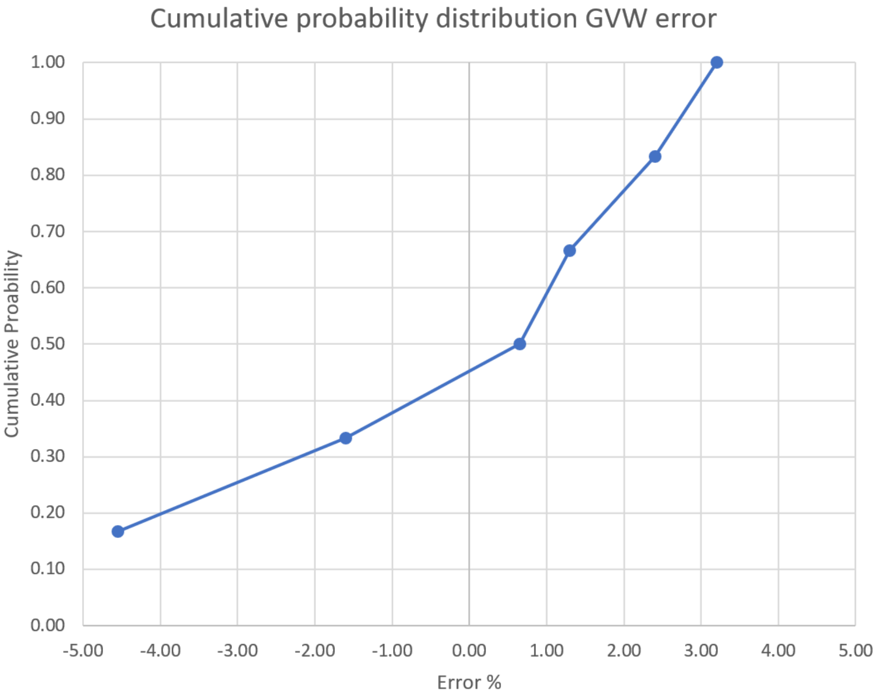

Figure 42 Plot of cumulative probability distribution in GVW error using C factor value average across two different known GVWs with 3 runs for each.

5.7 Axle detection

Axles detected from geophone data were compared with the axle configuration observed in the video footage. Table 13 shows the axle detection accuracy of the geophone sensor, which was 82% for 72 trucks.

Table 13 Results of axles detected compared to real number of axles.

Number of trucks	**Trucks with All axles detected**	**Trucks with one or more axles missing**	**Trucks with all axles correctly detected %**
72	59 trucks	13 trucks	82 %

5.7.1 Filter by GVW

As discussed in Field experiment 1, it was observed that the weights of trucks with empty or very light axles were not detected consistently; one of such trucks is shown in Figure 43. Due to this limitation of the methodology, empty tandem axles groups were filtered out. Based on the collected data, vehicles weighing greater than 150 kN exhibited consistent axle detection. Table 14 shows the performance of axle detection based on this filter, increasing the detection accuracy to 95%.

Figure 43 Photograph of an example of a lightly loaded truck.

Table 14 Results of axles detected with filter of GVW greater than 150 kN.

Number of trucks	Trucks with All axles detected	Trucks with one or more axles missing	Trucks with all axles correctly detected %
41	39 trucks	2 trucks	95 %

5.8 Axle spacings for test truck

Table 15 presents the axle spacings results for the calibration truck, calculated from geophone data, and compares them with the known axle spacings depicted in Figure 35 and Figure 36. The maximum absolute error for axles 1-2 was 0.42 meters in experiment 1 and 0.29 meters in experiment 2, with error percentages of ±8% and ±5% respectively. For axles 2-3, the maximum absolute error was 0.1 meters in experiment 1 and 0.14 meters in experiment 2, with error percentages of ±7% and ±11% respectively. These findings suggest that among the detected axles, the calculation of axle spacings is minimally affected by axle weights. However, it is crucial for axle loads to be sufficiently high to ensure accurate detection as discussed in Field experiment 2.

Table 15 Results of axle spacings performance.

Experiment 1		
	Axle 1-2	**Axle 2-3**
Real space	5.38 m	1.35 m
Error range	-0.22%, 7.8%	-6.5%, 2.4%
Average error	2.7%	-1.6%
Maximum Error value	0.42 m	-0.09 m

Experiment 2		
Real space	5.38 m	1.35 m
Error range	1.2%, 5.4%	-10.5%, 3.5%
Average error	3.2%	-2.6%
Maximum Error value	0.29 m	-0.14 m

Table 16 shows the performance metrics of the overall axle spacings calculation. Figure 44 shows the cumulative probability distribution for the measured errors in Axle spacings. For 16 samples, the error range is -10.52% to 7.8%, with 95% confidence interval being -2.4% to 3.2%.

Table 16 Performance metrics of Axle Spacings calculation

Error range	**-10.52% to 7.8%**
Average error	0.40%
Sample size	16
95% CI average error	(-2.4%, 3.2%)
Error Standard deviation	5.25%
95% CI standard deviation	(3.9%, 8.1%)

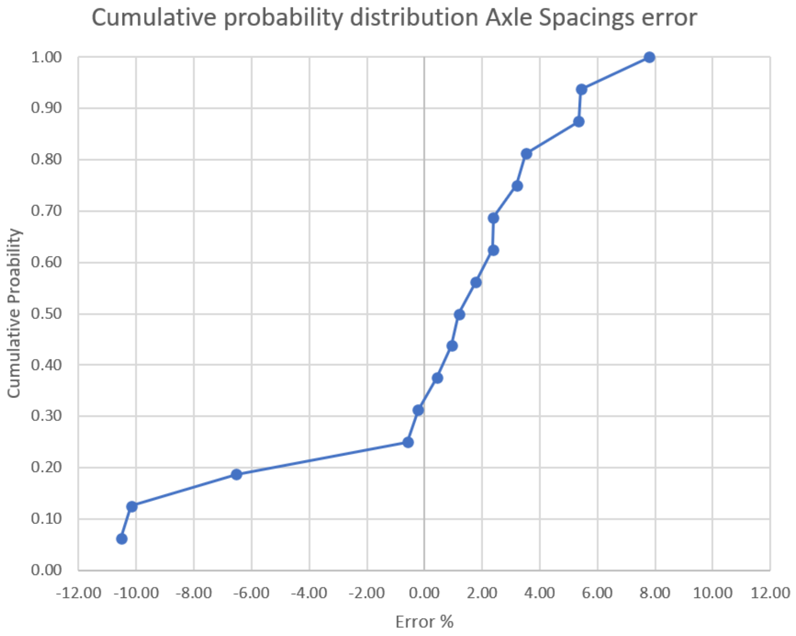

Figure 44 Plot of cumulative probability distribution in the Axle spacings errors as measured from geophone data against the known axle spacings for test truck.

5.9 Axle loads

Table 17 shows the results for the axle loads of the calibration truck as calculated using the described methodology compared to the real known axle loads shown in Figure 35 and Figure 36. The maximum absolute error for axles 1 was 3 kN with maximum error being ±5.3%, and the maximum absolute error for axles 2 and 3 was 1.5 kN with maximum error being ±3.2%.

Table 17 performance of the estimated loads for test truck.

Experiment 1				
Axle #	**Real load (kN)**	**Estimated load (kN)**	**Absolute error (kN)**	**Error %**
1	57	54	3	-5.26
2 and 3	34	37	3	8.82
Experiment 2				
1	61	63	2	3.28

2 and 3	46.5	45	1.5	-3.2

Table 18 shows the performance metrics of axle loads calculation and Figure 45 shows the cumulative probability distribution for the measured errors in Axle loads. For 8 samples, the error range is -4.97% to 10.48%. Due to lower sample size, 90% confidence level was calculated, and it is 1.05% to 8.6%.

Table 18 Performance metrics of axle loads calculation.

Error range	**-4.97% to 10.48%**
Average error	4.8%
Sample size	8
90% CI average error	(1.05%, 8.6%)
Error Standard deviation	5.66%
90% CI standard deviation	(4%, 10.2%)

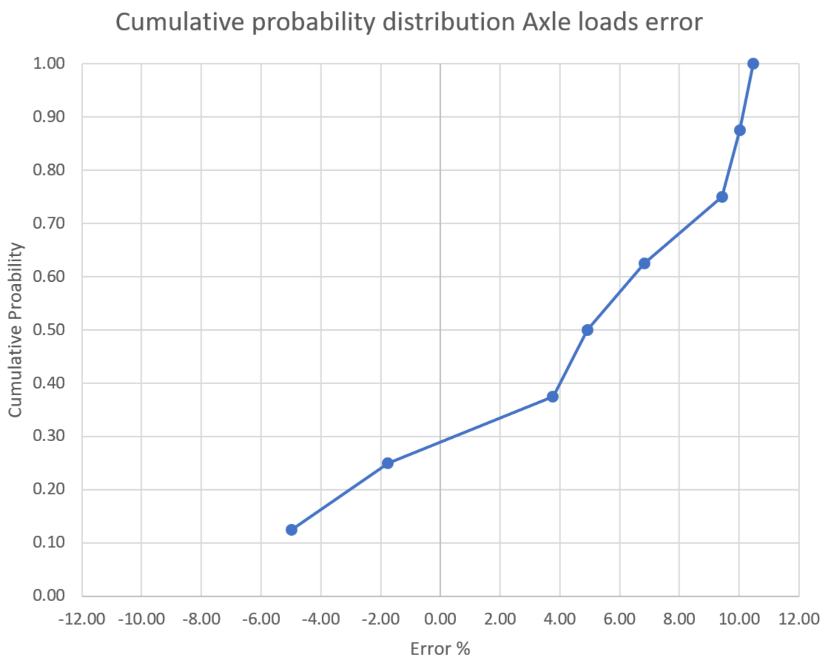

Figure 45 Plot of cumulative probability distribution in Axle load error as measured from data compared with known axle loads of the test truck with two different axle configurations.

5.10 Vehicles on the Non-Instrumented Span

As shown in Figure 4, only the eastbound lanes were instrumented in this methodology. However, the westbound lanes are also physically connected to the instrumented span and vehicles passing through this side. These vehicles are also observable on the sensors signals and influence the measurements of the methodology. Figure 46 shows a photograph of an example truck traveling westbound. Figure 47 shows the measured signals corresponding to this truck. It is important to note that no information about the axle configuration can be seen in the geophone signals for these vehicles.

Figure 46 Photograph of a truck travelling in the westbound lanes.

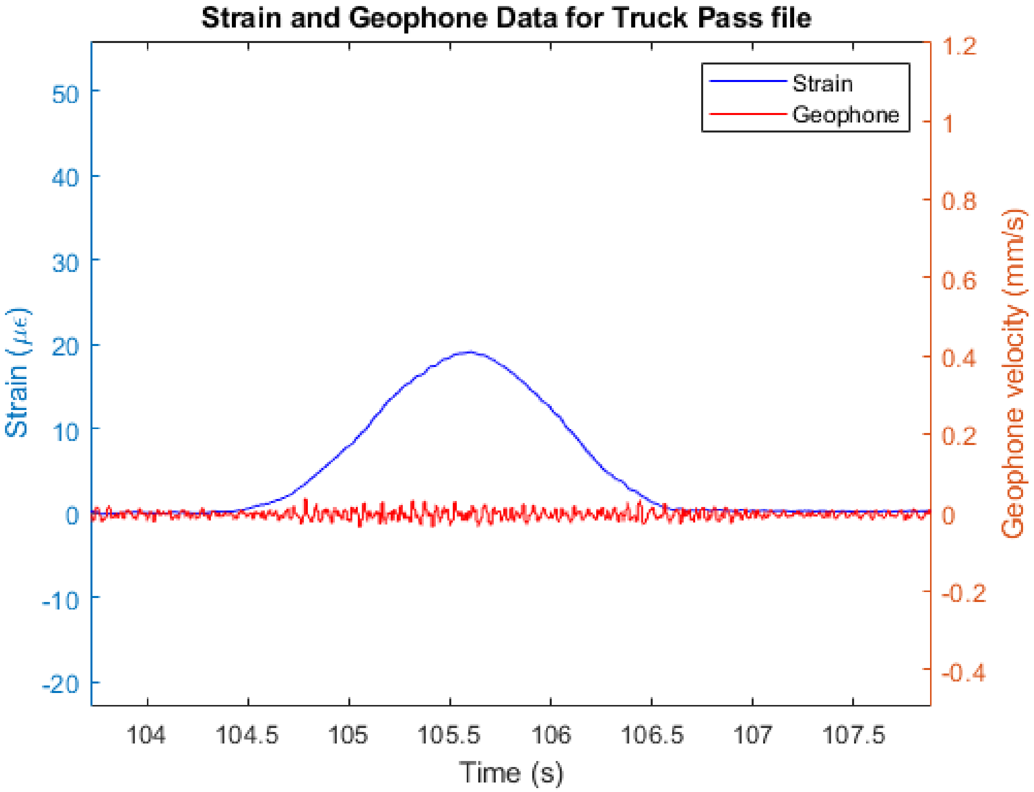

Figure 47 Captured data for this truck showing no information about axles.

6 DISCUSSION

This chapter goes through the entire analysis process discussed in the Data analysis chapter for one example truck. The process is shown with examples starting with the raw data to data pre-processing to vehicle properties extraction. Afterwards, suggestions are given for future improvements to the system, which could potentially improve the performance of vehicle properties extraction.

6.1 Walkthrough of an example

Figure 48 shows an 8-axle truck chosen to demonstrate the process of data analysis. The selected vehicle is an 8-axle B-double configuration (3-S3-S2) truck. It is subject to a length limit of 25 meters, axle load limits, and GVW limit of 62,500 kg or 613 kN on this highway. It was selected due to its large number of axles to demonstrate the process more clearly. The truck was traveling at regular traffic speeds and no specific identifying features were recorded.

Figure 48 Photograph of an 8-axle example truck.

Figure 49 (a) shows the raw data in voltages as captured by the sensors. Figure 49 (b) shows the data after pre-processing with highlighted peaks for the arrival time of each axle.

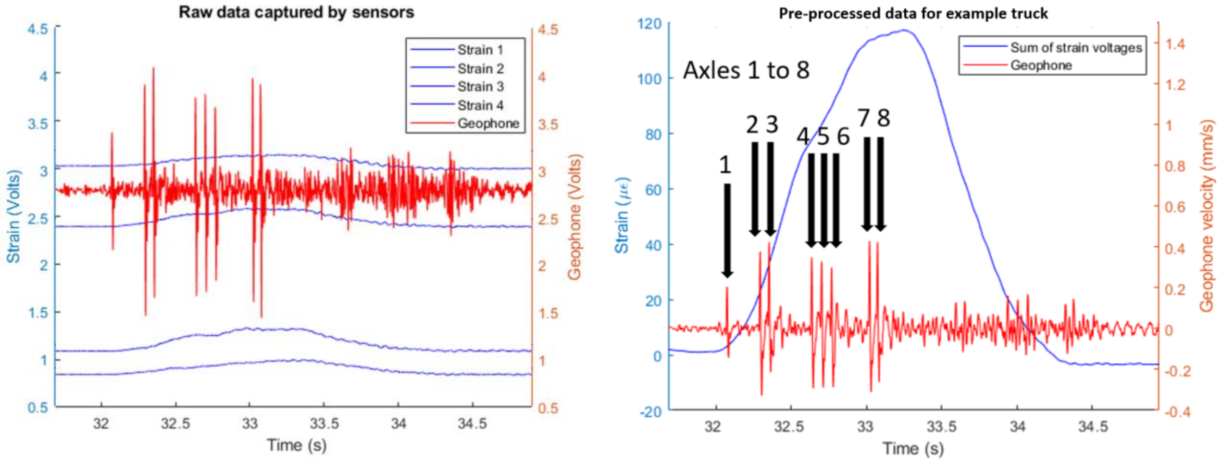

(a) Raw data recorded for example truck. *(b) Pre-processed data with axle peaks shown.*

Figure 49 Plots of raw and pre-processed data for the example truck.

Figure 50 shows the PCC history of arrival signal against the entire signal. It shows peaks at arrival time with perfect correlation and a peak at departure time with highest correlation as the arrival window overlaps with the departure window.

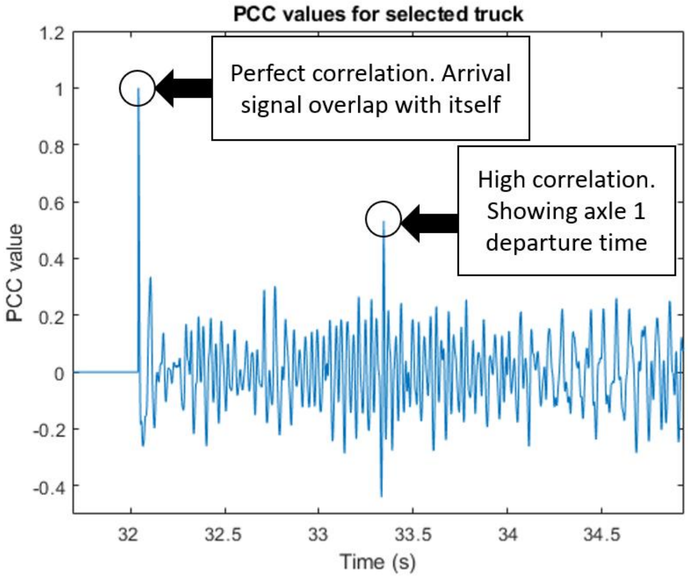

Figure 50 Plot of PCC values overtime showing peaks with high correlation for truck departure time.

Figure 51 shows the plot of processed data with velocity and departure window highlighted. The velocity was calculated to be 22.4 meters per second, which is within the legal limit on this highway.

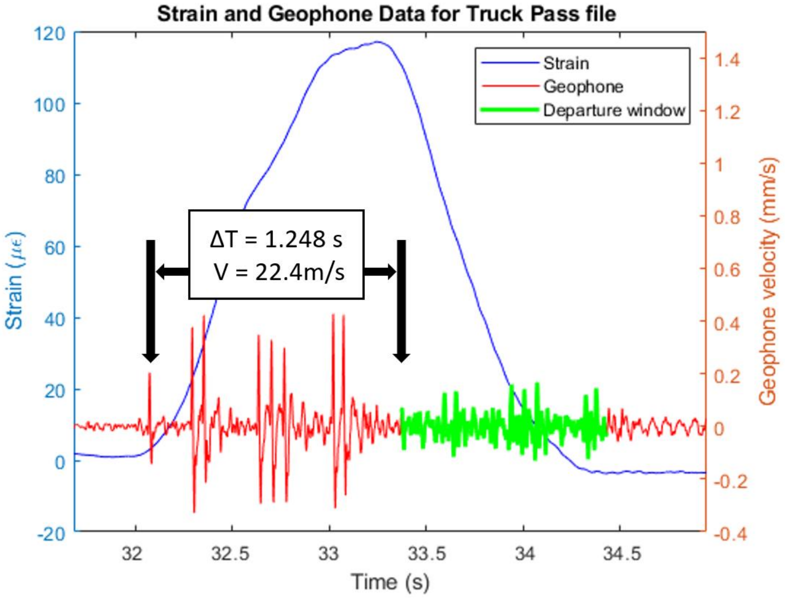

Figure 51 Plot of processed data showing velocity calculation and departure window highlighted.

6.1.1 Axle spacings

Table 19 shows the results for axle spacings for each of the 8 axles as calculated from the geophone signal.

Table 19 Result of axle spacings calculation for example truck.

	Axle 1-2	**Axle 2-3**	**Axle 3-4**	**Axle 4-5**	**Axle 5-6**	**Axle 6-7**	**Axle 7-8**
ΔT (s)	0.219 s	0.066 s	0.276 s	0.066 s	0.067 s	0.252 s	0.052 s
Distance (m)	4.93 m	1.48 m	6.18 m	1.48 m	1.5 m	5.6 m	1.16 m

Figure 52 shows the plot of GVW calculation and area under strain highlighted. The GVW was calculated to be 595 kN, which is within the legal limitations.

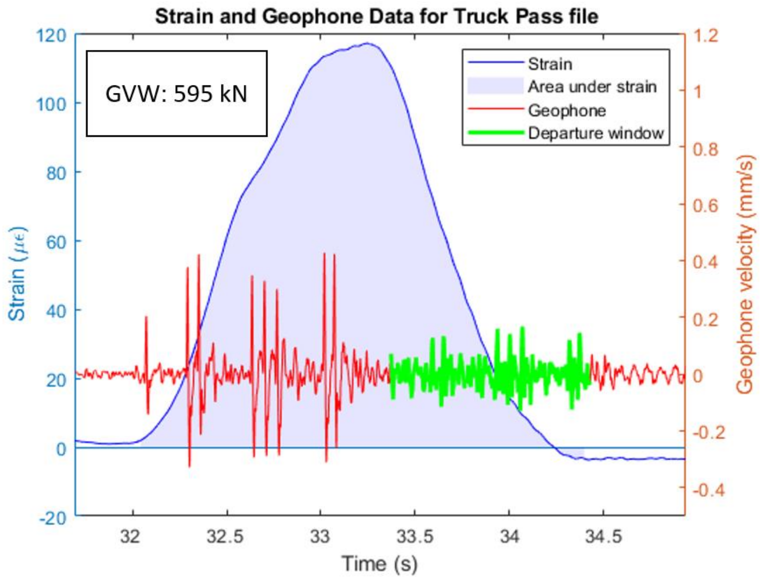

Figure 52 Plot of GVW calculation and area under strain highlighted.

6.1.2 Axle loads determination

Figure 53 shows the history of regression iterations fitting the theoretical strain of the vehicle with the detected axle configuration. Figure 53 (a) and (b) show the starting configuration. Figure 53 (c) and (d) show the update after 5 iterations. Finally, Figure 53 (e) and (f) show the results at iteration number 20.

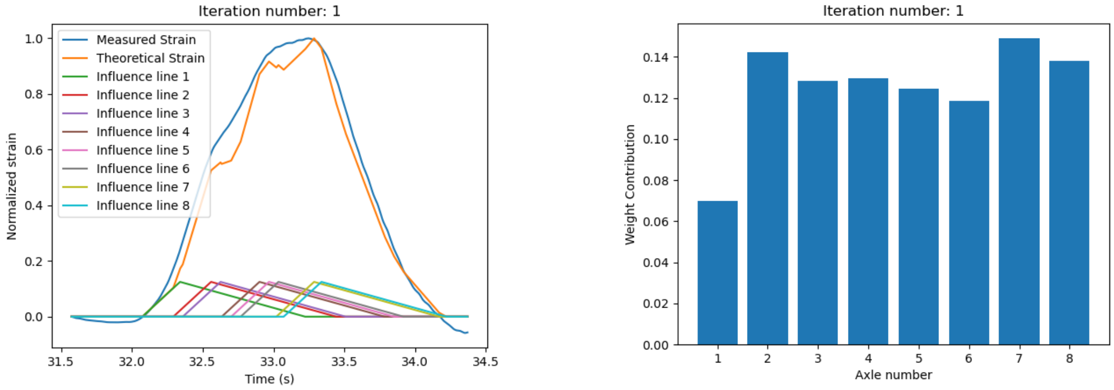

(a) Theoretical vs Measured strain at Iteration 1.

(b) Weights at iteration 1.

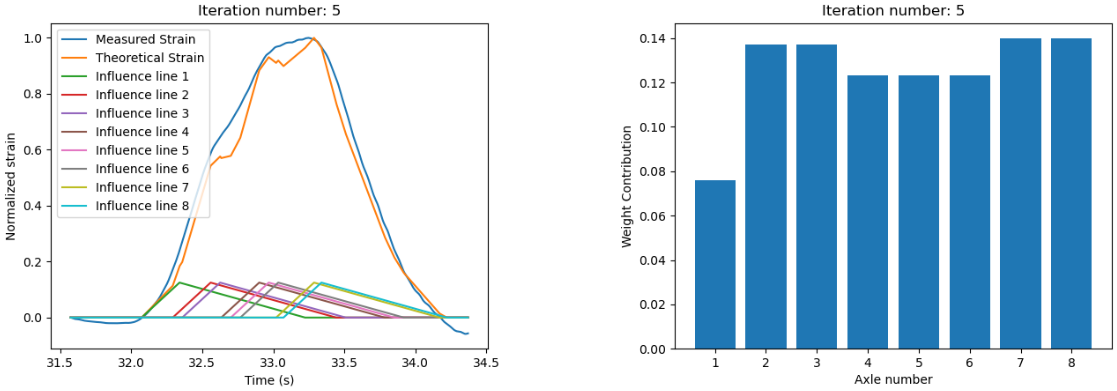

(c) Theoretical vs Measured strain at Iteration 5.

(d) Weights at iteration 5.

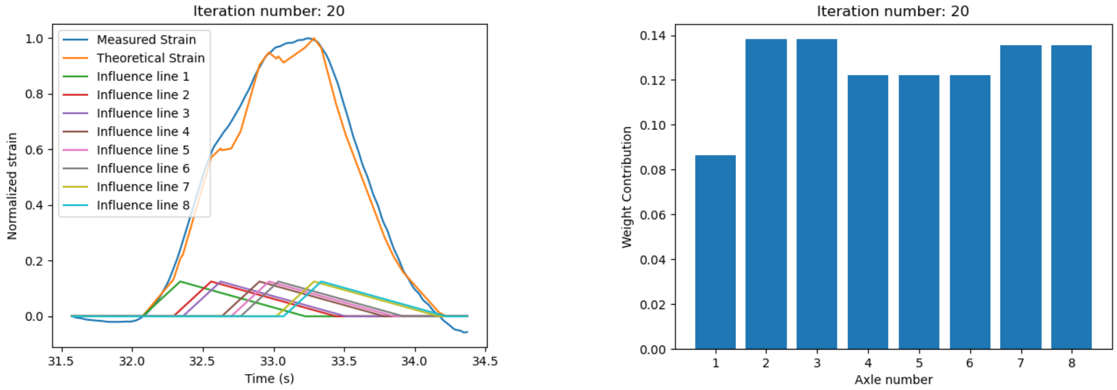

(e) Theoretical vs Measured strain at Iteration 20.

(f) Weights at iteration 20.

Figure 53 Regression performance over iterations

Figure 54 (a) shows the update history of weight parameters, and Figure 54 (b) shows the loss history of the theoretical strain vs measured strain. Figure 55 shows the results at the end of the regression analysis.

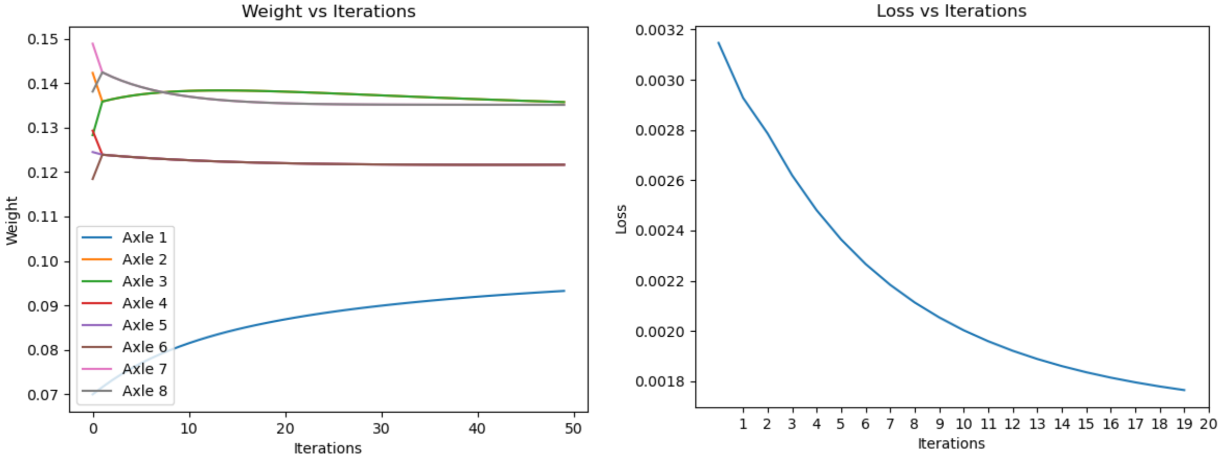

(a) Weights update history over iterations

(b) Loss update history over iterations

Figure 54 Updates history over 20 iterations.

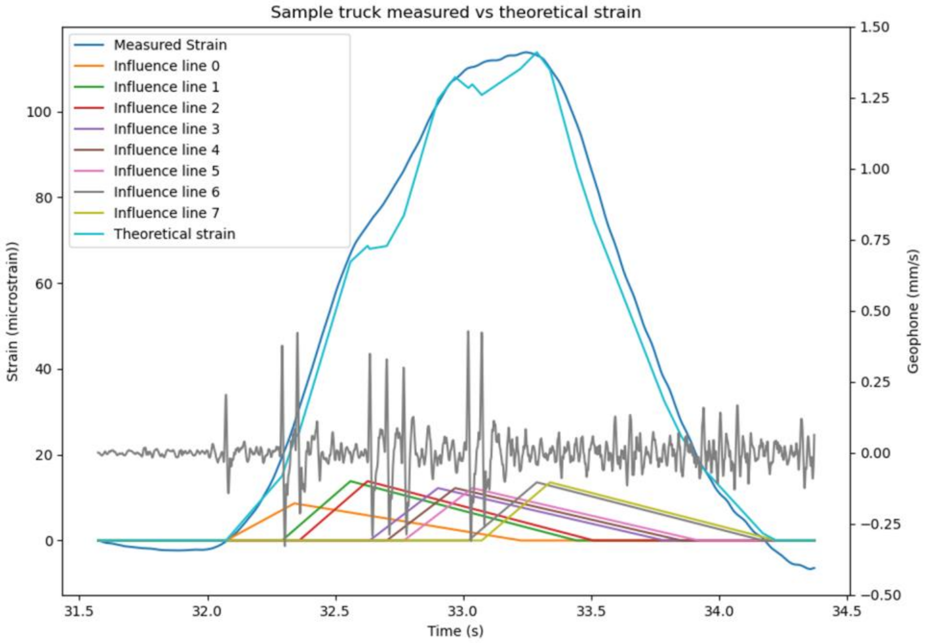

Figure 55 Plot of theoretical strain with weights from regression overlayed on measured strain.

6.1.3 Analysis results

Table 20 shows a summary of all the vehicle parameters extracted from the example truck.

Table 20 Results of analysis for example truck.

Axles detected	8
Velocity	22.4 m/s
GVW	595 kN
Load of Axle 1	51.4 kN
Loads of Axles 2 and 3	2 x 82.2 kN
Loads of Axles 4, 5 and 6	3 x 72.7 kN
Load of Axles 7 and 8	2 x 80.6 kN

6.2 Representing GVWs as equivalent length

While reporting on GVWs observed on a bridge, it becomes valuable to differentiate between vehicles with identical GVWs but distinct axle load distributions. Recent Advances in Bridges Engineering (Mufti, 2008) offers a practical method using equivalent length in chapter 1.2. It involves the concept of equivalent base length (Bm), representing axle weights as a uniformly distributed load (UDL) with the same total load W. The equation (11) is used for calculating Bm for an equivalent UDL.

$$B_m = \frac{4}{W}\sum_{i=1}^{N}|P_i x_i| - \frac{2(N-1)}{bNW^2}\left\{\sum_{i=1}^{N}(P_i x_i)\right\}^2 \tag{11}$$

Where W is the GVW, N is the number of axles, b is the base length, P_i and x_i are the i^{th} axle load and axle spacing from point load closest to the center of gravity.

Let's examine a 5-axle truck with GVW of 150 kN, featuring two distinct axle load configurations. In configuration (a), the middle two axles bear heavier loads, while configuration (b) distributes the load uniformly across all axles. Figure 56 provides a visualization of the equivalent base length for these two configurations, illustrating how the concept of equivalent base length aids in understanding axle load distributions for different configurations at the same GVW.

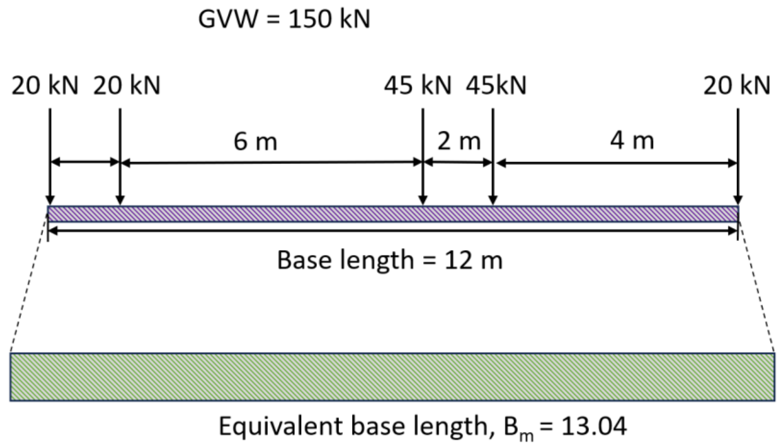

(a) Load concentrated on middle axles.

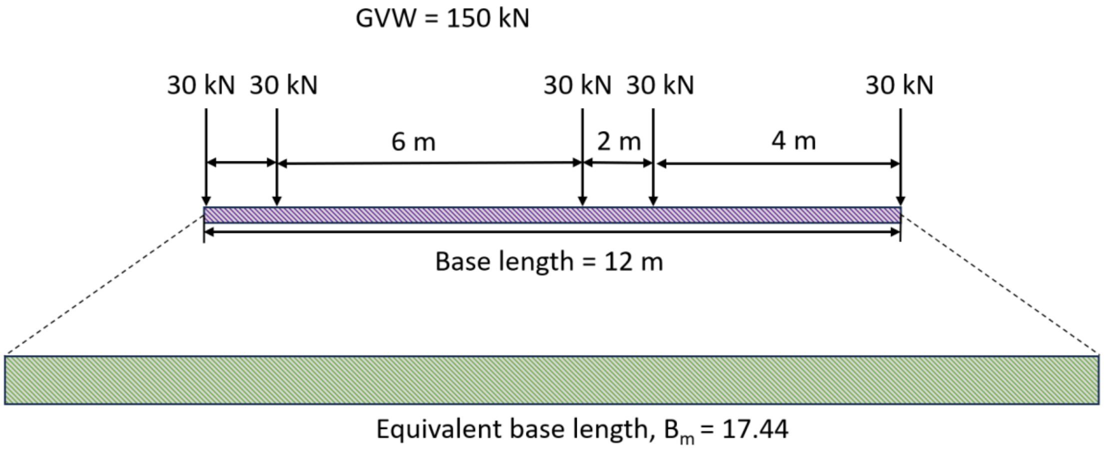

(b) Load evenly distributed.

Figure 56 Example of equivalent base lengths.

7 CONCLUSIONS

In conclusion, the developed methodology exhibits promising capabilities. However, there is room for improvement. Increasing the sample size will provide further confidence in the estimations. The system exhibited the following performance metrics.

- Velocity measurements exhibited an error ranging from -5% to 3.8%, achieving a 95% confidence interval of -0.4% to 0.54% and an R^2 value of 0.95, based on a sample size of 64 vehicles.
- GVW calculations displayed performance metrics with an error range of -4.6% to +3.2% and a 95% confidence interval spanning -2.7% to 3.2%, derived from 6 runs of known GVWs.
- Axle detection accuracy was determined to be 95%, demonstrated across a sample size of 41 trucks selected based on their GVW exceeding 150 kN.
- Axle spacings calculations showed an error range of -10.52% to 7.8%, with a 95% confidence interval of -2.4% to 3.2%, based on 16 samples of known values.
- Axle loads performance metrics, derived from 8 samples of known values, indicated an error range of -4.97% to 10.48%, with a 90% confidence level of 1.05% to 8.6%.

7.1 Limitations

Some limitations of the proposed methodology are stated below.

- Tandem axle groups with individual axles weighing less than 40kN were not consistently detected by the geophone sensor. Implying that the proposed methodology does not work consistently for empty or very lightly loaded trucks.

- The proposed methodology does not adjust for presence of other vehicles on the bridge span. Runs with multiple simultaneous vehicles were ignored in the performance metrics.
- The proposed methodology assumed velocity to be constant between when a vehicle enters and leaves the instrumented span.
- Since the strain signal has a moving average filter of 250 samples and the calculated influence lines are sharp and the normalization locks the peak of the strain shape to a maximum value of 1, it stands to reason that applying the same filter over the calculated influence line may reduce the positive error bias seen in Figure 45.

7.2 Future work

The following are some suggestions that could improve the performance of the methodology.

- Multiple Geophone Instrumentation: Placing geophones on all girders at both ends of the span can enhance axle detection, velocity measurement, and axle load estimation.
- Exploration of Alternative Regression Models: Investigating additional regression models with different loss functions could improve the methodology's performance.

7.2.1 Suggestions for Improved Vehicle Separation

Effectively distinguishing between simultaneous vehicles remains a persistent challenge in BWIM. Addressing this difficulty is crucial for accurate analysis, especially when different vehicles traverse an instrumented bridge span simultaneously. The following recommendations explore potential approaches to address this challenge.

Integration of Computer Vision: Enhance BWIM instrumentation by integrating cameras and developing image recognition capabilities. These cameras capture visual data, and the implemented image recognition algorithms can effectively identify, and track vehicles based on their visual features. This integration has the potential to be a reliable approach for vehicle separation, axle configuration, and overall analysis.

Improved sensor placements and algorithms: While the current methodology utilizes a single geophone, optimizing vehicle separation may involve deploying a geophone on each girder at both ends of the span. This enhanced sensor arrangement can provide richer information, potentially leading to the development of algorithms capable of differentiating individual vehicle characteristics, even in scenarios involving overlapping traffic.

8 REFERENCES

Law, S. S., Bu, J. Q., Zhu, X. Q., & Chan, S. L. (2004). Vehicle axle loads identification using finite element method. Engineering Structures, 26(8), 1143-1153.

Fu, G., & Hag-Elsafi, O. (2000). Vehicular overloads: Load model, bridge safety, and permit checking. Journal of Bridge Engineering, 5(1), 49-57.

Jacob, B., & Feypell-de La Beaumelle, V. (2010). Improving truck safety: Potential of weigh-in-motion technology. IATSS research, 34(1), 9-15.

Haghani, R., Al-Emrani, M., & Heshmati, M. (2012). Fatigue-prone details in steel bridges. Buildings, 2(4), 456-476.

Mufti, A. A., Bakht, Baidar., & Jaeger, L. G. (2008). Recent advances in bridge engineering. JMBT Structures Research

Archilla, A. R., & Madanat, S. (2000). Development of a pavement rutting model from experimental data. Journal of transportation engineering, 126(4), 291-299.

Rashidi, M., Mohammadi, M., Sadeghlou Kivi, S., Abdolvand, M. M., Truong-Hong, L., & Samali, B. (2020). A decade of modern bridge monitoring using terrestrial laser scanning: Review and future directions. Remote Sensing, 12(22), 3796.

Lydon, M., Taylor, S. E., Robinson, D., Mufti, A., & Brien, E. J. O. (2016). Recent developments in bridge weigh in motion (B-WIM). Journal of Civil Structural Health Monitoring, 6, 69-81.

Moses, F. (1979). Weigh-in-motion system using instrumented bridges. Transportation Engineering Journal of ASCE, 105(3), 233-249.

Helmi, K., Bakht, B., & Mufti, A. (2014). Accurate measurements of gross vehicle weight through bridge weigh-in-motion: a case study. Journal of Civil Structural Health Monitoring, 4(3), 195-208.

Algohi, B., Mufti, A., & Bakht, B. (2020). BWIM with constant and variable velocity: theoretical derivation. Journal of Civil Structural Health Monitoring, 10, 153-164.

Bakht, B., Mufti, A., Jaeger, L. G., & Helmi, K. (2013). Determining gross vehicle weight by BWIM. ISIS Canada Resource Centre, University of Manitoba, Canada.

Faraz, S. (2020). Experimental and Field Investigation of a Bridge- Weigh-in-Motion (BWIM) System.

Mirzaei, M. (2022). Enhancing bridge weigh-in-motion system by accurate observation of the velocity and axle spacings of moving truck using a geophone sensor.

Peters, R. J. (1986). CULWAY, an unmanned and undetectable highway speed vehicle weighing system. In Australian Road Research Board Proceedings.

Richardson, J., Jones, S., Brown, A., O’Brien, E., & Hajializadeh, D. (2014). On the use of bridge weigh-in-motion for overweight truck enforcement. International Journal of Heavy Vehicle Systems, 21(2), 83-104.

Paul, D., & Roy, K. (2023). Application of bridge weigh-in-motion system in bridge health monitoring: a state-of-the-art review. Structural Health Monitoring, 14759217231154431.

Znidaric, A., Lavric, I., Kalin, J. (1998). Extension of Bridge WIM Systems to Slab Bridges. Pre-Proceedings of Second European Conference on Weigh-in-Motion of Road Vehicles, 139-152.

McNulty, P., O’Brien, E., J. (2003). Testing of Bridge Weigh-in-Motino System in Sub-Arctic Climate. Journal of Testing and Evaluation, 31(6), 1-10.

O’Brien, E., J., Quilligan, M., J., Karoumi, R. (2006). Calculating an Influence Line from Direct Measurements. Bridge Engineering, Proceedings of the Institution of Civil Engineers, 159(BE1), 31-34.

Quilligan, M., Karoumi, R., O’Brien, E., J. (2002). Development and Testing of a 2-Dimensional Multi-Vehicle Bridge-WIM Algorithm. Proceedings of the Third International Conference on Weigh-in-Motion, 199-208.

Zhao, H., Uddin, N., O’Brien, E., J., Shao, X., Zhu, P. (2014). Identification of Vehicular Axle Weights with a Bridge Weigh-in-Motion System Considering Transverse Distribution of Wheel Loads. Journal of Bridge Engineering, 19(3), 04013008.

Kalin, J., Znidaric, A., Lavric, I. (2006). Practical Implementation of Nothing-on-the-Road Bridge Weigh-in-Motion System. Proceedings: Ninth International Symposium for Road Transport Technology, Penn State State College, Pennsylvania, USA.

Dempsey, A. T., Jacob, B., Carracilli, J. (1998). Orthotropic Bridge Weigh-in-Motion for Determining Axle and Gross Vehicle Weights. Second European Conference on Weigh-in-Motion of Road Vehicles, 435-444.

Ojio, T., Yamada, K., Shinkai, H. (2000). BWIM Systems Using Truss Bridges. Bridge Management 4, 378-385.

Ojio, T., Yamada, K. (2002). Bridge Weigh-in-Motion Systems Using Stringers of Plate Girder Bridges. Pre-Proceedings of the Third International Conference on Weigh-in-Motion, 209-218.

Ojio, T., Carey, C. H., OBrien, E. J., Doherty, C., & Taylor, S. E. (2016). Contactless bridge weigh-in-motion. Journal of Bridge Engineering, 21(7), 04016032.

He, W., Ling, T., OBrien, E. J., & Deng, L. (2019). Virtual axle method for bridge weigh-in-motion systems requiring no axle detector. Journal of Bridge Engineering, 24(9), 04019086.

Gonçalves, M. S., Carraro, F., & Lopez, R. H. (2021). A gradient based optimization procedure for finding axle weights in probabilistic bridge weigh-in-motion method. Canadian Journal of Civil Engineering, 48(5), 570-574.

Yu, Y., Cai, C. S., & Deng, L. (2017). Vehicle axle identification using wavelet analysis of bridge global responses. Journal of Vibration and Control, 23(17), 2830-2840.

Lydon, M., Robinson, D., Taylor, S. E., Amato, G., Brien, E. J., & Uddin, N. (2017). Improved axle detection for bridge weigh-in-motion systems using fiber optic sensors. Journal of Civil Structural Health Monitoring, 7, 325-332.

Mustafa, S., Sekiya, H., Hirano, S., & Miki, C. (2021). Iterative linear optimization method for bridge weigh-in-motion systems using accelerometers. Structure and Infrastructure Engineering, 17(9), 1245-1256.

Brincker, R., Lagö, T. L., Andersen, P., & Ventura, C. (2005). Improving the classical geophone sensor element by digital correction. In Conference Proceedings: IMAC-XXIII: A Conference & Exposition on Structural Dynamics. Society for Experimental Mechanics.

Sirohi, J., & Chopra, I. (2000). Fundamental understanding of piezoelectric strain sensors. Journal of intelligent material systems and structures, 11(4), 246-257.

Cohen, I., Huang, Y., Chen, J., Benesty, J., Benesty, J., Chen, J., ... & Cohen, I. (2009). Pearson correlation coefficient. Noise reduction in speech processing, 1-4.